

Date of publication xxxx 00, 0000, date of current version xxxx 00, 0000.  
Digital Object Identifier 10.1109/ACCESS.2017.Doi Number

# Electronically tunable ACO based Fuzzy FOPID Controller for effective Speed Control of Electric Vehicle

MARY ANN GEORGE<sup>1</sup>, Student, Member, IEEE, DATTAGURU V. KAMAT<sup>2</sup>, Sr. Member, IEEE, and CIJI PEARL KURIAN<sup>3</sup>, Sr. Member, IEEE

<sup>1,2</sup>Department of Electronics and Communication Engineering, Manipal Institute of Technology, Manipal Academy of Higher Education (MAHE), Manipal 576104, India

<sup>3</sup>Department of Electrical and Electronics Engineering, Manipal Institute of Technology, Manipal Academy of Higher Education (MAHE), Manipal 576104, India

Corresponding author: Dattaguru V. Kamath (e-mail: dv.kamath@manipal.edu).

**ABSTRACT** The phenomenal growth of the Electric Vehicle (EV) technology demands efficient and intelligent control strategies for the propulsion system. In this work, a novel fuzzy fractional order PID (FOPID) controller using Ant Colony Optimization (ACO) algorithm has been proposed to control EV speed effectively. The controller parameters and the fuzzy logic controller's membership functions are tuned and updated in real-time using the multi-objective ACO technique. The proposed controller's speed tracking performance is verified using the new European driving cycle (NEDC) test in the MATLAB-Simulink platform. The proposed controller outperforms the ACO-based fuzzy integer-order PID (IOPID), FOPID, and traditional IOPID controllers. The sensitivity analysis confirms the robustness of the proposed controller for varying parameters of the EV model. The stabilization of EV speed in the presence of external disturbance is also confirmed. In the proposed work, an attempt is made to analyze the system's stability using Matignon's theorem, considering the linearized EV model. The proposed controller gives optimum speed tracking performance compared to the Genetic Algorithm (GA) and the Particle Swarm Optimization (PSO) based fuzzy FOPID controllers. Additionally, the optimized fuzzy FOPID controller is realized using a second-generation current conveyor with extra inputs (EX-CCII) and fractional-order capacitors with electronic tunability. The controller circuit's performance evaluation is carried out in the Cadence Analog Design Environment using GPDK 180 nm CMOS process.

**INDEX TERMS** Ant Colony Optimization, Electric Vehicle, Multi-objective optimization, Fuzzy FOPID, Second-generation current conveyor with extra inputs.

## I. INTRODUCTION

The rise in environmental concerns and demand for fossil fuel resources has necessitated incorporating electric vehicle (EV) technology. In the recent past, EVs have gained popularity concerning their high efficiency, low maintenance cost, and easy operations [1], [2]. The emerging trend in EVs has led to massive pollution reduction and better sustainability in urban cities. The propulsion system has been an integral part in deciding the overall performance of EV. The researchers at industrial and academic levels have primarily focused on developing controls for the propulsion system of the EV [3]. Efficient performance and desirable energy management are the two key parameters that require intensive and focused

investigations. The controller should provide the maximum speed with low tracking error and energy consumption [4]. The EV system is highly non-linear, time-dependent, and uncertain due to the varying road conditions, motor parameters, and external disturbances. Hence, designing a controller that eliminates the external disturbances and handling uncertainties with low control signal has become a challenge [5].

The conventional PID controllers are generally used in various industrial applications due to their simplicity and ease of tuning [6], [7]. However, they do not perform effectively at varied operating conditions and do not assure desired dynamic performance [8]. The use of fuzzy logic control with PID

controllers enhances the classical PID controller's performance with self-tuning features [9]–[13]. Fuzzy controllers have been widely used in controlling EV systems. Khatun et al. [14] developed a fuzzy controller to control the EV antilock braking system by compensating for the non-linear dynamics. A fault-tolerant fuzzy controller can raise EV's initial torque with variable characteristics of speed and high efficiency [15].

The emergence of fractional calculus has led to the development of fractional order PID controller that offers two additional degrees of freedom, the non-integer order of the integrator and the differentiator stages [16]–[18]. The non-integer order controller provided better servo, regulatory performance, and robustness compared to its integer-order counterparts. The significant benefits of fractional order controllers are their efficacy, flexibility in system modeling, and design performance [19], [20].

The artificial intelligence (AI) based controllers have gained importance due to their satisfactory performance in various motor control applications, including speed assessment and torque ripple minimization [21]. However, AI-based controllers suffer from drawbacks, such as large data requirements, extended learning, and training duration. A fuzzy logic controller is a powerful tool that can integrate human reasoning into the controller design [13]. The fuzzy controllers can operate in linear and non-linear systems without considering their accurate mathematical models [22]. The fuzzy controllers outperform other controllers in complex and non-linear systems for which good practical knowledge exists. The accuracy of fuzzy logic controllers depends on the type and number of fuzzy membership functions and fuzzy rules. At present, the optimization techniques explored with fuzzy logic control have gained massive attention in various industrial applications due to their high-quality results, high efficiency, ability to adapt, and high accuracy. Hence, an optimal fuzzy logic controller can be designed by utilizing optimization techniques such as Genetic Algorithm (GA) [23], Particle Swarm Optimization (PSO) [24], Backtracking Search Algorithm (BSA) [25], Bee Colony Optimization (BCA) and differential evolution (DE) [26].

Das et al. [27] presented a GA-based optimized fuzzy FOPID controller, which could provide a better set-point tracking with a significant compromise in rejecting the load disturbance. Kumar et al. [28] investigated the design of a cascade fractional-order fuzzy PI and PD controller for a hybrid electric vehicle based on a multi-objective genetic algorithm. The fuzzy FOPID controllers have been widely used in various applications such as vibration isolation structure [29], pneumatic pressure system [30], pumped storage unit regulating system [31], and Automatic Generation Control (AGC) for electrical power systems [8], [13]. It is evident from the literature that combining fuzzy logic with fractional operators could further improve the feedback control system's robustness. Additionally, introducing an adaptive or self-

tuning feature can even enhance the controller capability and system performance.

The majority of the controllers in current industries have been implemented in the digital form using PLC or microprocessors. However, the digital controllers have low speed and low memory capacity, making them unsuitable for fast processes such as speed control of EVs and chemical reactions [32]. The digital implementation also suffers from high power consumption related to the analog-to-digital (A/D) converter.

There have been several works on the analog circuit realization of the FOPID controller reported in the literature, using analog blocks like Operational Transconductance Amplifier (OTA) [32], [33], CCII [34], Voltage Differencing Current Conveyor (VDCC) [35]. Most of these circuits suffer from drawbacks, such as a high number of active/ passive elements [32], [33], and lack of electronic tunability [34].

#### **A. MOTIVATION AND RESEARCH GAP**

The majority of the reported work on tuning the fuzzy logic input and output scaling factors focus on GA [23], PSO [23], [24], and Cuckoo algorithm [36]. Apart from the scaling factors, the position of the input and output membership functions plays a vital role in the fuzzy logic controller [37]. Hence, it is worth noting that the tuning of membership function can significantly enhance the system's performance. The Ant Colony Optimization (ACO) algorithm is preferred to optimize the controller parameters and tune the membership functions due to its numerous advantages compared to other optimization algorithms such as GA and PSO [38]. The ACO algorithm is a meta-heuristic approach that offers high robustness, better reliability, greater flexibility, fast convergence, easy implementation, and fewer optimization parameters [38]–[41]. It is also capable of combining with other algorithms. It is well suited for feature selection and parameter tuning with better global search ability. It is suitable for dynamic applications and can quickly adapt to changes.

The analog circuit realization of the FOPID controller involves the realization of fractional-order capacitors, which are not yet available commercially. The behavior of the fractional-order capacitors can be emulated using the RC ladder/ tree structures [42] and multiple-loop-feedback structures [43]. Considering the RC structures' greater energy consumption and a more significant number of active element count required for the multiple-loop-feedback structures, a better solution using a resistor less and energy-effective structure to realize the fractional-order capacitors is deemed necessary.

#### **B. CONTRIBUTION AND PAPER ORGANIZATION**

1. This work focuses on the efficient design and circuit realization of a fuzzy FOPID controller for EV speed control. The optimization of the input /output scaling factors, antecedent part of input membership function,

and coefficients of the consequent parts of the Takagi-Sugeno fuzzy inference system is performed using the ACO algorithm.

2. The proposed optimization is expected to minimize the multi-objective function to improve the time-domain performance indices. The novel controller's ability to reject disturbances and provide robustness to uncertainties and parameter variations has also been investigated in this study. The controller facilitates the fastest tracking with minimum overshoot and low values of time-domain performance indices.
3. The stability analysis and eigenvalue analysis of the proposed ACO-based fuzzy controller and EV model is carried out.
4. The performance of the proposed controller is also compared with GA and PSO-based fuzzy FOPID controllers.
5. The suggested controller is realized using a single EX-CCII, which provides a simultaneous realization of the fractional-order integrator and the differentiator stages of various orders and the unity gain frequencies. An OTA-based resistorless topology is employed to emulate the fractional-order capacitors used to realize the fractional-order differentiator and the integrator stages. This study anticipates gaining some valuable and novel insights into the effective real-time performance of the EV propulsion system to find broad applications in the ongoing efforts in sustainable growth.

The paper has been organized as follows: Section II describes the mathematical model of the EV. Section III gives the fuzzy FOPID controller structure with details of the two-dimensional rule base and membership functions. It also explains the formulation of a multi-objective function along with the ACO algorithm used for optimization. The circuit realization of the fuzzy FOPID controller using the EX-CCII with electronic tuning features is presented in Section IV. Section V compares the performances of the fuzzy IOPID and the fuzzy FOPID controllers for set-point tracking, disturbance rejection, and uncertainties. It also presents the results of circuit simulation, and the concluding remarks are outlined in Section VI.

## II. MATHEMATICAL MODEL OF ELECTRIC VEHICLE

The EV mainly comprises a battery unit, controller, and electric motors connected to the vehicle through the transmission unit. The EV system dynamics has two parts: vehicle and motor dynamics. The electric vehicle system modeling involves the balancing of all the forces acting on a running vehicle. There are mainly four types of forces, namely rolling friction ( $F_{rr}$ ), aerodynamic drag force ( $F_{ad}$ ), gravitational force ( $F_g$ ), and force due to vehicle acceleration ( $F_a$ ), as shown in Figure 1.

Hence, the total traction force ( $F_t$ ) acting on a vehicle is given by

$$F_t = F_{rr} + F_{ad} + F_g + F_a \quad (1a)$$

$$= \mu_{rr}mg + 0.5\rho AC_d v^2 + mgsin\varphi + m \frac{dv}{dt} \quad (1b)$$

where  $m$  is the mass of the electric vehicle,  $g$  is the gravity acceleration,  $v$  the driving velocity of the vehicle,  $\mu_{rr}$  the rolling resistance coefficient,  $\rho$  the air density,  $A$  the frontal area of the vehicle,  $C_d$  the drag coefficient and  $\varphi$  the hill-climbing angle. Table I describes the EV parameters and specifications.

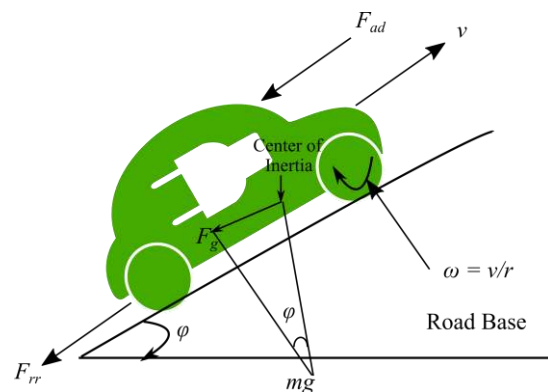


FIGURE 1. External forces acting on a running EV.

The resultant force  $F_t$  produces a torque  $T_L$  to the driving motor and is given by

$$T_L = F_t \times \frac{r}{G} \quad (2)$$

where  $r$  is the EV tire radius and  $G$  the gearing ratio. The non-linear model of the DC motor [44] is given by

$$\frac{di}{dt} = \frac{1}{(L_a + L_f)} \{V - (R_a + R_f)i - L_{af}i\omega\} \quad (3a)$$

$$\frac{d\omega}{dt} = \frac{1}{J} \{L_{af}i^2 - B\omega - T_L\} \quad (3b)$$

where  $i$  is considered the armature and field current,  $\omega$  the angular speed of the motor,  $L_a$  the armature inductance,  $R_a$  the armature resistance,  $L_f$  the field winding inductance,  $R_f$  the field winding resistance,  $L_{af}$  the mutual inductance among the field and armature windings,  $B$  the viscous coefficient,  $J$  the moment of inertia of the motor,  $T_L$  the external torque and  $V$  the input voltage.

Hence, the driving velocity of the vehicle  $v$  is given by

$$v = \omega \times \frac{r}{G} \quad (4)$$

Therefore, by combining the vehicle and the motor dynamics, the overall EV model is given by

$$\frac{di}{dt} = \frac{1}{(L_a + L_f)} \{V - (R_a + R_f)i - L_{af}i\omega\} \quad (5a)$$

$$\frac{d\omega}{dt} = \frac{1}{J + m(r/G)^2} \left\{ L_{af} i^2 - B\omega - \frac{r}{G} (\mu_{rr} mg + 0.5\rho AC_d v^2 + mgsin\varphi) \right\} \quad (5b)$$

TABLE I  
EV PARAMETERS AND SPECIFICATIONS [45]

Symbol	Value	Symbol	Value
$L_a + L_f$	6.008 mH	$m$	800 kg
$R_a + R_f$	0.12 $\Omega$	$A$	1.8 m <sup>2</sup>
$L_{af}$	1.766 mH	$\rho$	1.25 (kg/m <sup>3</sup> )
$i$	78 A (250 max)	$C_d$	0.3
$V$	0 ~ 48 V	$\mu_{rr}$	0.015
$B$	0.0002 N.M.s	$\varphi$	0°
$J$	0.05 kg m <sup>2</sup>	$G$	11
$\omega$	25 km/h	$r$	0.25 m

The equations (5a) and (5b) of the EV can be represented in Simulink, as shown in Figure 2.

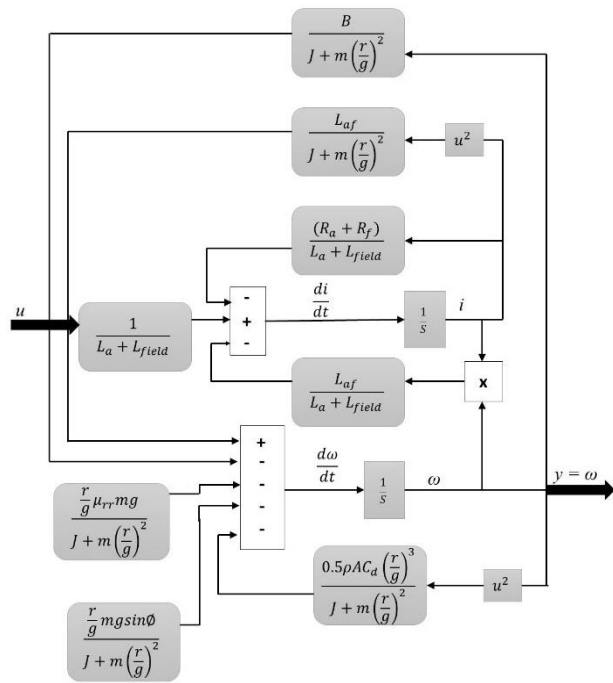


FIGURE 2. Representation of an EV system in Simulink.

The non-linear model in (5) can be converted into state-space form as

$$\dot{X} = f(X) + g(X)u \quad (6)$$

where

$$X = \begin{bmatrix} x_1 \\ x_2 \end{bmatrix} = \begin{bmatrix} i \\ \omega \end{bmatrix}$$

$$f(X) = \begin{bmatrix} -\frac{R_a + R_f}{L_a + L_f} x_1 - \frac{L_{af}}{L_a + L_f} x_1 x_2 \\ \frac{1}{J + m(r^2/G^2)} \left\{ L_{af} x_1^2 - Bx_2 - \frac{r}{G} (\mu_{rr} mg + \frac{1}{2} \rho AC_d \frac{r^2}{G^2} x_2^2 + mgsin\varphi) \right\} \end{bmatrix}$$

$$g(X) = \begin{bmatrix} 1 \\ L_a + L_f \\ 0 \end{bmatrix}, h(X) = x_2$$

### III. DESIGN OF A FUZZY FRACTIONAL ORDER PID

During the last few decades, fractional calculus has been widely used in solving control problems [46]. Fractional calculus is an essential branch of mathematics that uses non-integer order powers of integration and differential operators. The differ-integration operator  ${}_a D_t^r$  represents a fractional order differentiation and integration as in (7)

$${}_a D_t^r \begin{cases} \frac{d^r}{dt^r} & r > 0 \\ 1 & r = 0 \\ \int_a^t (dt)^{-r} & r < 0 \end{cases} \quad (7)$$

where  $r \in R$  is the order of the operation and  $\alpha, t$  the lower and the upper limits.

Several definitions have been reported in the literature to define the differ-integration operator, such as Reimann-Liouville, Grunwald-Letnikov, Caputo, Cauchy integral formula. The fractional-order operator  $s^r$  can be approximated to an integer order rational function using Oustaloup's approximation method [47]. Oustaloup's method is based on a recursive distribution of poles and zeros for a frequency range of  $[\omega_b, \omega_h]$ . Oustaloup's approximation for the analog filter takes the form

$$s^r \cong C \prod_{k=-N}^N \frac{s + \omega_k'}{s + \omega_k} \quad (8a)$$

where  $r \in [-1, 1] \subseteq R$

The expressions for zeros, poles and gain are given by

$$\omega_k' = \omega_b \left( \frac{\omega_h}{\omega_b} \right)^{\frac{k+N+0.5(1-r)}{2N+1}} \quad (8b)$$

$$\omega_k = \omega_b \left( \frac{\omega_h}{\omega_b} \right)^{\frac{k+N+0.5(1+r)}{2N+1}} \quad (8c)$$

$$C = \omega_h^r$$

Here,  $\omega_b$  is the lower transitional frequency, and  $\omega_h$  is the higher transitional frequency. The unity gain frequency  $\omega_o$  is calculated by  $\omega_o = \sqrt{\omega_b \omega_h}$  and order of the transfer function is  $n = 2N + 1$ , which can only be an odd-order approximation. By selecting  $N = 2$  and the frequency band as  $[10^{-3}, 10^3]$ , the analog filter order turns out to be equal to 5.

The expression of the FOPID controller is given as

$$C(s) = K_p + \frac{K_i}{s^\lambda} + K_d s^\mu \quad (9)$$

where  $K_p$  is the proportional gain,  $K_i$  the integral gain,  $K_d$  the derivative gain,  $\lambda$  the order of the integrator stage, and  $\mu$  the order of the differentiator stage. The time-domain expression of the control output of the FOPID controller is given by

$$u(t) = K_p e(t) + K_i D^{-\lambda} e(t) + K_d D^\mu e(t) \quad (10)$$

where  $e(t)$  is the tracking speed error.

The structure of a fuzzy FOPID controller is shown in Figure 3. The error ( $e$ ) and the fractional derivative of error ( $de$ ) are the two inputs to the fuzzy FOPID, and  $o$  is the output of the fuzzy FOPID controller.

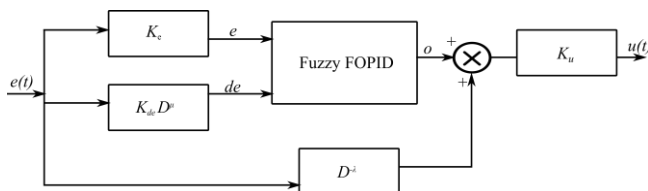


FIGURE 3. Structure of fuzzy FOPID controller.

By using linear transformation for the control output  $u(t)$  in Figure 3, we get

$$u(t) = (K_e e(t) + K_{de} D^\mu e(t) + D^{-\lambda} e(t)) K_u \quad (11)$$

By comparing (10) and (11), the gain expressions can be given as

$$K_p = K_e K_u \quad (12a)$$

$$K_d = K_{de} K_u \quad (12b)$$

$$K_i = K_u \quad (12c)$$

where  $K_e$ ,  $K_{de}$  are the input scaling factors and  $K_u$  the output scaling factor.

Here, a Takagi-Sugeno type fuzzy inference system (FIS) is used. The FIS has three blocks, i.e., fuzzification, decision-making logic with rule base, and defuzzification, as shown in Figure 4. In the fuzzification stage, the crisp input values are converted to a linguistic variable using a triangular membership function, with a 50% overlap. The triangular membership function is described as

$$f(x, a, b, c) = \begin{cases} 0, & x \leq 0 \\ \frac{x-a_k}{b_k-a_k}, & a_k \leq x \leq b_k \\ \frac{c_k-x}{c_k-b_k}, & b_k \leq x \leq c_k \\ 0, & c_k \leq x \end{cases} \quad (13)$$

where  $a_k$ ,  $c_k$  denote the feet and  $b_k$  the peak of the triangular membership function. The distribution of membership functions for the input variables  $e$  and  $de$  are shown in Figures 5 (a) and 5 (b). The input variables have five fuzzy sets: Negative Big (NB), Negative Medium (NM), Zero (Z),

Positive Medium (PM), and Positive Big (PB). Figure 6 shows the distribution of the output membership function. The fuzzy IF-THEN rule describes a condition that relates the linguistic variables and fuzzy sets to the output [48]. Table II describes the 25 IF-THEN rules used in this work. The Takagi-Sugeno type FIS gives a crisp output, either a linear combination of the inputs or a constant. Hence, it is considered as a weighted average defuzzification process. The proposed scheme of the fuzzy FOPID controller for the EV system is illustrated in Figure 4. The Takagi-Sugeno FIS consumes less time compared to that of a Mamdani fuzzy system [9].

TABLE II  
RULE BASE FOR FUZZY FOPID CONTROLLER

e/de	NB	NM	Z	PM	PB
NB	NB	NB	PM	NM	NM
NM	NB	NM	Z	Z	Z
Z	NB	NM	Z	PM	PB
PM	Z	Z	Z	PM	PB
PB	PM	PM	PM	PB	PB

The input and output scaling factors ( $K_e$ ,  $K_{de}$ ,  $K_u$ ), adjustable parameters of input membership function ( $X$ ,  $Y$ ), coefficient of the consequent part ( $Z$ ), the order of integrator ( $\lambda$ ), and order of differentiator ( $\mu$ ) are varied to achieve an optimal solution and improve the speed tracking performance of electric vehicle system.

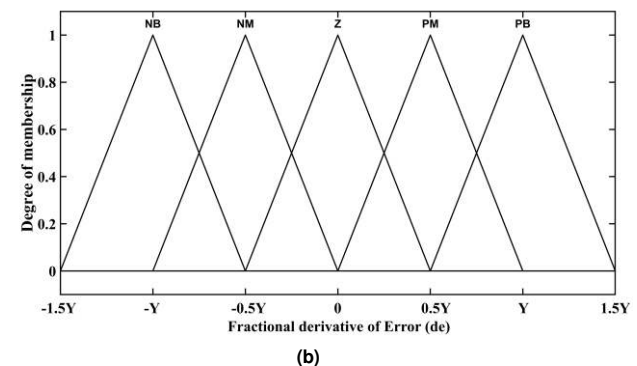
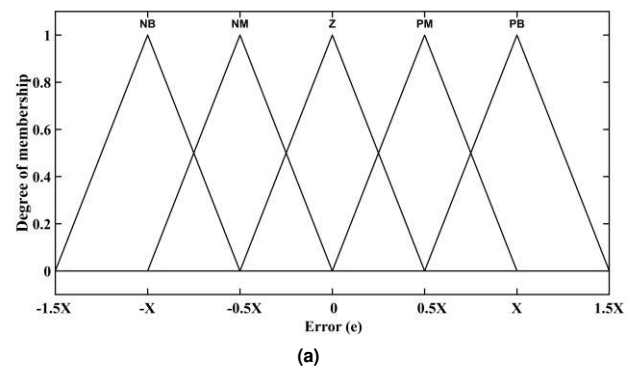
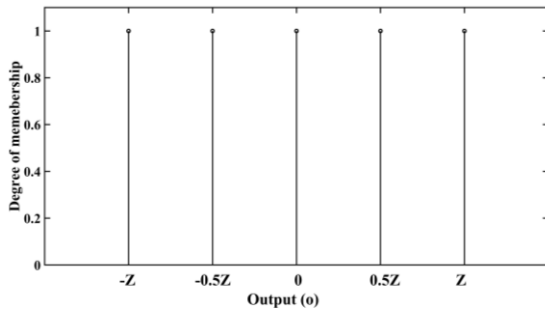


FIGURE 5. Distribution of input membership function (a) error ( $e$ ), (b) fractional derivative of error ( $de$ ).



**FIGURE 6.** Distribution of the output of Takagi-Sugeno type FIS.

The fuzzy FOPID controller is tuned using the ACO algorithm, and its performance is compared with other optimization algorithms in the MATLAB-Simulink platform.

### A. ANT COLONY OPTIMIZATION (ACO)

The ACO is one of the robust and adaptive algorithms used to solve optimization problems based on the natural behavior of the ants [49]. The optimal solution can be determined when the ants' colony communicates with each other using an indirect method called the *pheromone decomposition*. The shortest distance from the initial state to the destination is found using a sequence of neighboring states. This algorithm can find the optimal solution faster when a higher number of pheromones are released. The pheromone matrix, which is used to determine the optimal solution, is  $\psi = \psi_{ab}$ . The initial state of the pheromone matrix is given by

$$\psi_{ab} = \psi_0 \quad \forall(a, b) \quad (14)$$

where  $\psi_0 > 0$ . The probability ( $P_{a,b}^Y$ ) of selecting node  $a$  at node  $b$  is given as

$$P_{a,b}^Y = \frac{[\psi_{ab}(t)]^\alpha [\eta_{ab}]^\beta}{\sum_{a,b \in T^Y} [\psi_{ab}(t)]^\alpha [\eta_{ab}]^\beta} \quad (15)$$

where  $T^Y$  defines the path executed at a given time by an ant ( $Y$ ),  $\alpha$  and  $\beta$  are the constants that determine the relative impact of the pheromones and the heuristic factors on ants' decision. The heuristic factor  $\eta_{ab}$  is given by

$$\eta_{ab} = \frac{1}{\text{distance between nodes } a \text{ and } b} \quad (16)$$

ACO Algorithm
Initialize the pheromone trail and parameters
Generate initial population size of ants
Evaluate the initial population according to fitness function
Find the best solution of the population
<b>While</b> not terminated
<b>Do until</b> each ant completely build a solution
Local trial update
<b>End Do</b>
Update the pheromone and probability
Evaporate the pheromones
Determine the best global ant
<b>End while</b>
Output the global best solution

**FIGURE 7.** Pseudocode for ACO algorithm.

The quality of pheromone  $\Delta\psi_{ab}^Y$  at each path is defined as

$$\Delta\psi_{ab}^Y = \begin{bmatrix} L^{best} \\ L^Y \\ 0 \end{bmatrix} \quad (17)$$

where  $L^{best}$  is the best solution in the current iteration and  $L^Y$  is the value of the objective function determined by an ant ( $Y$ ). A phenomenon known as pheromone evaporation is adopted to delete the previous pheromones when a better optimal solution is reached.

The expression for pheromone evaporation is given as

$$\psi_{ab}(t) = \rho \psi_{ab}(t-1) + \sum_{Y=1}^{NY} \Delta\psi_{ab}^Y(t) \quad (18)$$

where  $\rho$  ( $0 < \rho \leq 1$ ) is the evaporation rate, and  $NY$  denotes the number of ants. Figure 7 shows the pseudocode for the ACO algorithm.

### B. FORMULATION OF OBJECTIVE FUNCTION FOR TUNING

A controller can be optimal when its control parameters are adjusted such that the cost function is minimized. In multi-objective optimization, the cost function is a weighted sum of two or more objective functions. During optimization, it is crucial to minimize both the error index and the control signal. This optimization type can reduce the control signal's value, preventing the actuator's integral wind-up and saturation. In this study, five performance indices have been considered as follows:

$$J_1 = ITSE + ISCO = \int_0^\infty t e^2(t) dt + ISCO \quad (19a)$$

$$J_2 = ITAE + ISCO = \int_0^\infty t |e(t)| dt + ISCO \quad (19b)$$

$$J_3 = IAE + ISCO = \int_0^\infty |e(t)| dt + ISCO \quad (19c)$$

$$J_4 = ISE + ISCO = \int_0^\infty e^2(t) dt + ISCO \quad (19d)$$

$$J_5 = ITSE + ITAE + IAE + ISE + ISCO \quad (19e)$$

$$ISCO = \int_0^\infty u^2(t) dt \quad (19f)$$

where  $e(t)$  is the error signal,  $u(t)$  is the control signal,  $ITSE$  is the integral time square error,  $ITAE$  is the integral time absolute error,  $IAE$  is the integral absolute error,  $ISE$  is the integral square error, and  $ISCO$  is the integral of the squared control signal. Each of these performance indices has certain advantages in the control system design [50]. These performance indices are considered as the objective function for tuning, ensuring stability and better speed tracking performance when there is sudden load disturbance, parameter variation, and reference speed variation.

The ACO algorithm minimizes the objective function  $J_i$  ( $i = 1, 2, 3, 4, 5$ ) to produce the optimally tuned input and output scaling factors, integral-differential orders, and adjustable

parameters of membership functions of the fuzzy FOPID controller with a low control signal and error-index.

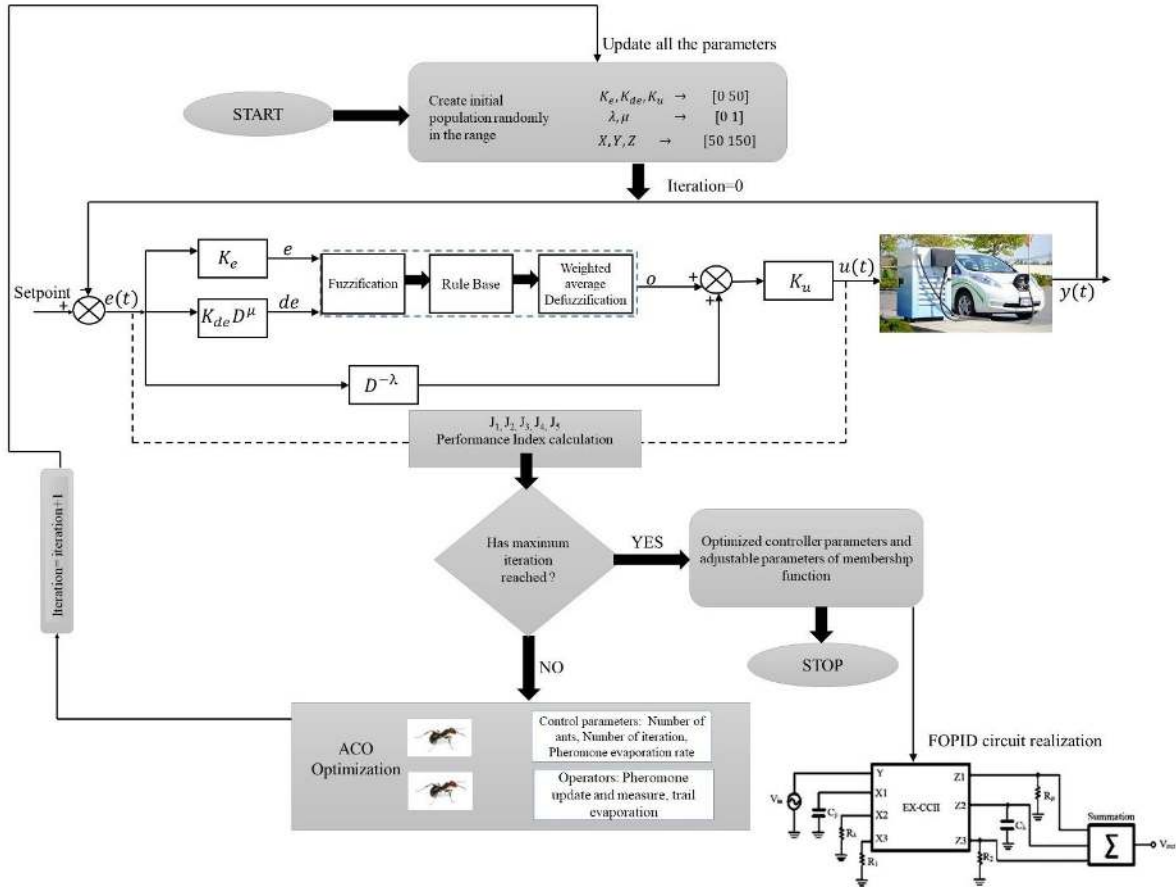


FIGURE 4. Block diagram of the proposed optimal fuzzy FOPID controller scheme for EV speed control.

#### IV. REALIZATION OF FOPID CIRCUIT USING EX-CCII

The optimum fractional PID controller can be realized using the extra-X second-generation current conveyor (EX-CCII) [34]. The main advantage of this structure is that a single active element is used to realize the controller, and the fractional-order differentiator and the integrator stages of any order can be implemented using the structure, as shown in Figure 8.

The terminal properties of EX-CCII are given by

$$\begin{aligned} V_{X1} &= V_{X2} = V_{X3} = V_Y \\ i_{Z1} &= i_{X1}, i_{Z2} = i_{X2}, i_{Z3} = i_{X3} \\ R_Y &\rightarrow \infty \end{aligned} \quad (20)$$

where  $V_{Xk}$  ( $k = 1, 2, 3$ ) are the voltages at input terminals  $Xk$ ,  $V_Y$  is the voltage at terminal  $Y$ ,  $i_{Zk}$  ( $k = 1, 2, 3$ ) are the currents at terminal  $Zk$  and  $i_{Xk}$  ( $k=1, 2, 3$ ) are the currents at terminals  $Xk$ .

The FOPID controller expression derived from applying terminal properties of EX-CCII in Figure 8 is given as

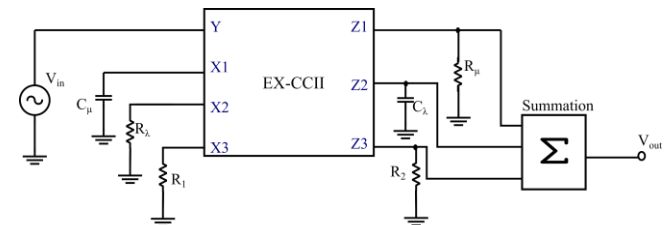


FIGURE 8. Realization of the FOPID controller using EX-CCII [34].

$$C(s) = \frac{R_2}{R_1} + \frac{1}{R_\lambda C_\lambda s^\lambda} + R_\mu C_\mu s^\mu \quad (21)$$

Here,  $C_\lambda$  and  $C_\mu$  are the pseudo-capacitance with units  $Farad/sec^{1-\lambda}$  and  $Farad/sec^{1-\mu}$ .

By comparing (21) and (9), we get

$$K_p = \frac{R_2}{R_1}, K_i = \frac{1}{R_\lambda C_\lambda}, K_d = R_\mu C_\mu \quad (22)$$

The fractional-order capacitors are approximated using the modified Oustaloup's approximation and realized using the RC Valsa network, as shown in Figure 9.

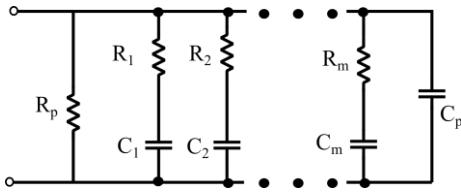


FIGURE 9. Valsa RC network.

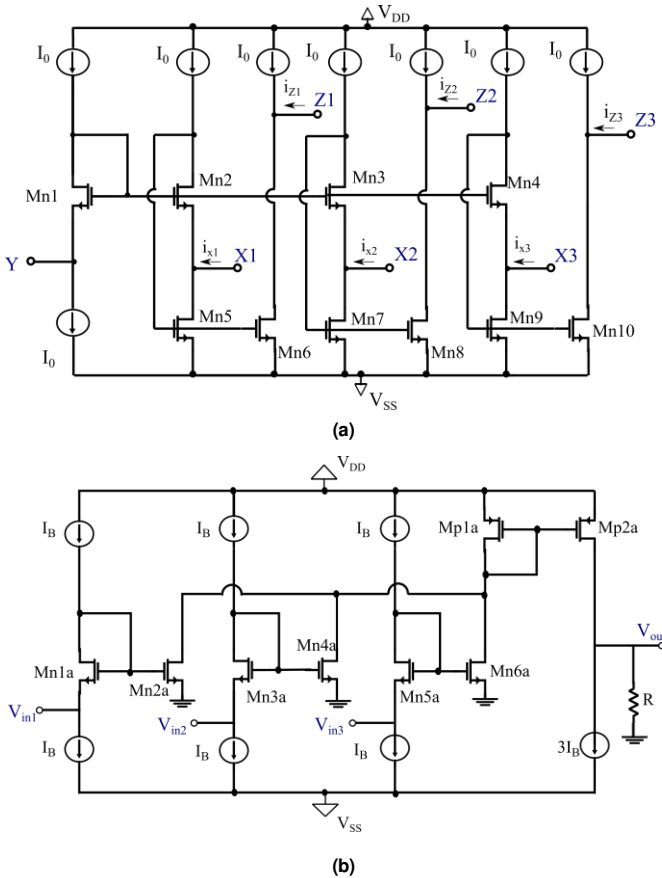


FIGURE 10. CMOS circuit of (a) three input EX-CCII, (b) three input summation stage [34].

The details of the multi-functional EX-CCII analog block and the three-input summation stage have been described in [34]. Figure 10 illustrates the CMOS realization of the three-input EX-CCII and the three-input summation stage. The EX-CCII circuit provides an accurate voltage conveying from terminal Y to terminals X1, X2, and X3. The currents from terminals X1, X2, and X3 are copied to terminals Z1, Z2, and Z3, respectively. The minimum supply voltage required is  $V_{THn} + 2V_{DS, sat}$ .

As the EX-CCII analog blocks are not available commercially, the FOPID controller circuit can be realized using CCII/CFOA integrated circuit (IC) AD844, as shown in Figure 11.

The output expression for the summation stage, shown in Figure 10 (b), is given as

$$V_{out} = g_m R (V_{in1} + V_{in2} + V_{in3}) \quad (23)$$

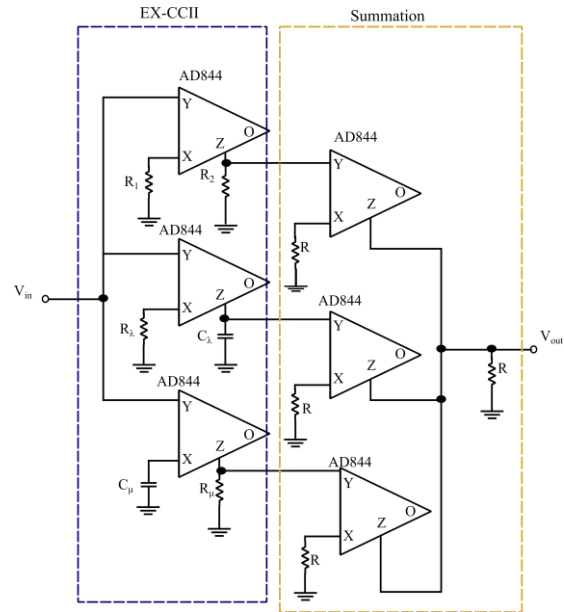


FIGURE 11. FOPID controller circuit using IC AD844 (current feedback operational amplifier).

Here,  $g_m$  is the transconductance of the transistors Mn1a-Mn6a and the resistance  $R = 1/g_m$ .

The electronic tunability of the EX-CCII based FOPID controller circuit in Figure 8 can be achieved by replacing all the passive grounded and floating resistors using operational transconductance amplifier (OTA) simulated resistors [51], [52], as shown in Figure 12 (a) and (b), respectively. This circuit offers benefits such as electronic tunability, wide bandwidth, simple design, and a wide range of resistance between  $50 \text{ M}\Omega$  and  $1 \text{ k}\Omega$ .

Assuming matched transistors, in Figure 12, the expression for current  $I_1$  is given by

$$I_1 = -I_2 = G_m(V_1 - V_2) \quad (24)$$

where  $V_1, V_2$  are the input voltages of the transconductance amplifier and  $G_m$  is the transconductance.

The resistance  $R$  and  $R_{12}$  can be found as

$$R = \frac{V_1}{I_1} = \frac{1}{\sqrt{\beta} I_{Bias}} \quad (25a)$$

$$R_{12} = \frac{V_1 - V_2}{I_1} = \frac{V_2 - V_1}{I_2} = \frac{1}{\sqrt{\beta} I_{Bias}} \quad (25b)$$

where  $I_{Bias}$  is the input biasing current  $\beta$  is the transconductance parameter of the MOS differential pair.



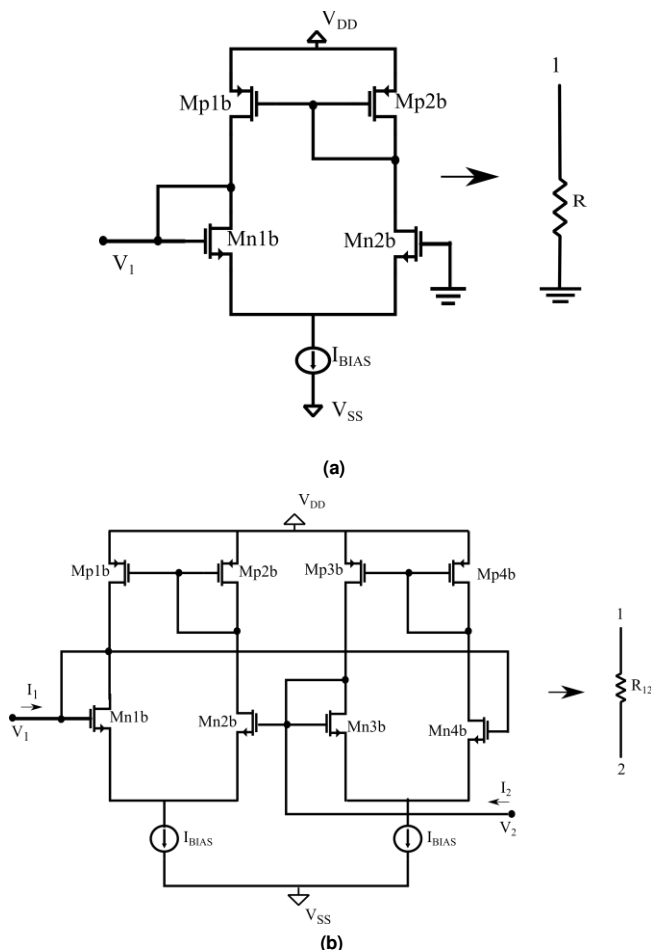


FIGURE 12. CMOS circuit of an electronically tunable resistor using OTA (a) grounded type, (b) floating type.

## V. RESULTS AND DISCUSSION

The optimal fuzzy FOPID controller for EV speed control shown in Fig. 4 is simulated using MATLAB-Simulink and Cadence Virtuoso Analog Design Environment. This section demonstrates the superiority of the ACO-based fuzzy FOPID controller over fuzzy IOPID controller, FOPID, and conventional IOPID controller through simulation of the EV system's speed tracking performance.

The parameters selected for ACO are given in Table III. The ACO minimizes the objective function (19a)-(19e) to determine the fuzzy controllers' optimal control parameters. Table IV shows the fuzzy FOPID and fuzzy IOPID controller parameters obtained after optimization considering various objective functions. Here,  $X$ ,  $Y$  are the antecedent values, and  $Z$  the value of the consequent.

Figure 13 illustrates the non-linear surface plot of the fuzzy IOPID and fuzzy FOPID obtained after ACO by minimizing the  $J_1, J_2, J_3, J_4, J_5$  objective functions. It shows the input and output relationship of the fuzzy logic controller. Here, the three axes are the error ( $e$ ), the fractional derivative of error ( $de$ ), and the output ( $o$ ) of the Takagi-Sugeno FIS. It illustrates

that the distribution of  $e$ ,  $de$ , and the coefficient of the consequent part of the output varies during the optimization. The blue and orange colour plots represent the output surface plot of fuzzy IOPID and fuzzy FOPID, respectively.

TABLE III  
PARAMETERS FOR ACO

Parameter	Value
Iteration	100
No. of ants	100
$\alpha$	0.8
$\beta$	0.2
$\rho$	0.7
Population	100
$K_e, K_{de}, K_u$	[0 50]
$\lambda, \mu$	[0 1]
$X, Y, Z$	[50 150]

Four operating scenarios are considered to validate the effectiveness and robustness of the proposed controllers, namely set-point tracking, disturbance rejection, noise suppression, and sensitivity analysis. This section also presents the stability analysis and eigenvalue analysis of the EV system. The performance comparison of the proposed scheme with other existing controllers is also described in this section.

**a. Set-Point Tracking:** The New European Driving Cycle (NEDC) test is performed to validate the fuzzy FOPID controller's performance. The NEDC has been commonly used to test the light-weighted EVs in Europe and India [53]. The maximum speed of the NEDC cycle is 120 km/h, as shown in Figure 14. The proposed fuzzy FOPID controller and fuzzy IOPID controller's performance to track the NEDC test is compared and illustrated in Figure 15 (a). It also shows the speed tracking performance of an ACO-based IOPID and FOPID controller. The proposed controllers' effectiveness is demonstrated by plotting the error signals and controller effort for each controller, as shown in Figure 15 (b) and 15 (c), respectively. As it can be inferred, while the IOPID controller produces the highest control effort and error signal, fuzzy FOPID generates the lowest control effort and error signal making its performance superior to others.

Table V summarizes the performance parameters of fuzzy FOPID and fuzzy IOPID controllers for various objective functions. The time-domain specifications such as settling time, rise time, percentage overshoot, steady-state error, and the performance indices such as  $ITSE$ ,  $ITAE$ ,  $IAE$ ,  $ISE$ , and  $J_5$  are compared for both controllers. Critical examination reveals that the fuzzy FOPID controllers' performance is far better than the fuzzy IOPID controllers with high accuracy, less settling time, percentage overshoot, steady-state error, and error indices. It also shows that the  $J_5$  optimized controllers have superior performance compared to  $J_1, J_2, J_3$ , and  $J_4$  optimized controllers.

The multi-objective optimization can result in solutions called the Pareto optimal solutions or non-dominant solutions. Figure 16 shows the distribution of the non-dominant solutions in the 4-dimensional Pareto optimal front ( $ITAE$ ,  $IAE$ ,  $ITSE$ ,  $ISE$ ) using multi-objective ACO. Here,  $J_5$  multi-objective function is chosen, and the resulting convergence graph of multi-objective ACO for 100 generations is illustrated in Figure 17.

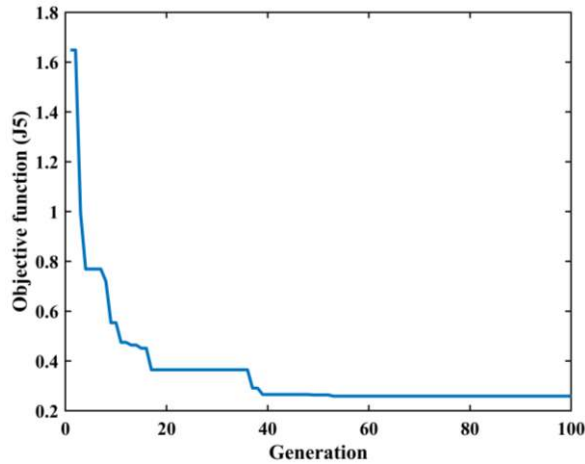


FIGURE 17. Convergence graph of ACO.

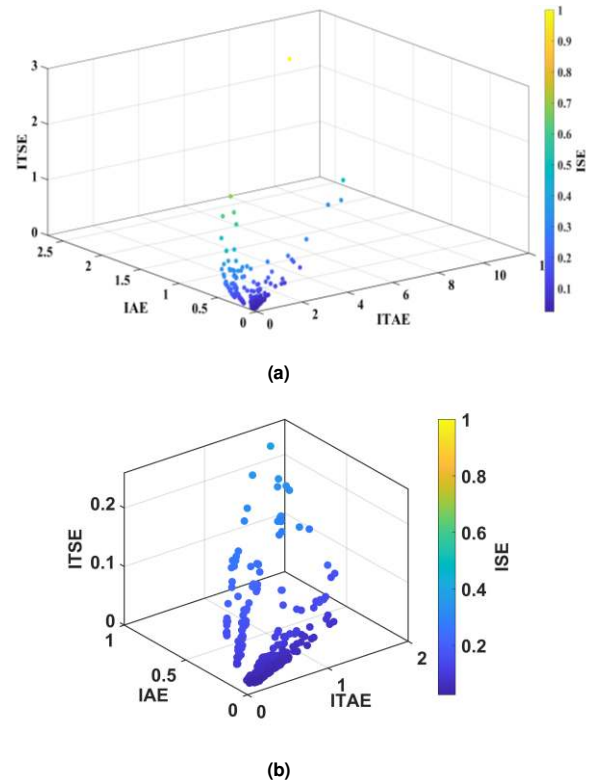


FIGURE 16. (a) 4D Pareto front using multi-objective ACO, (b) Zoomed plot.

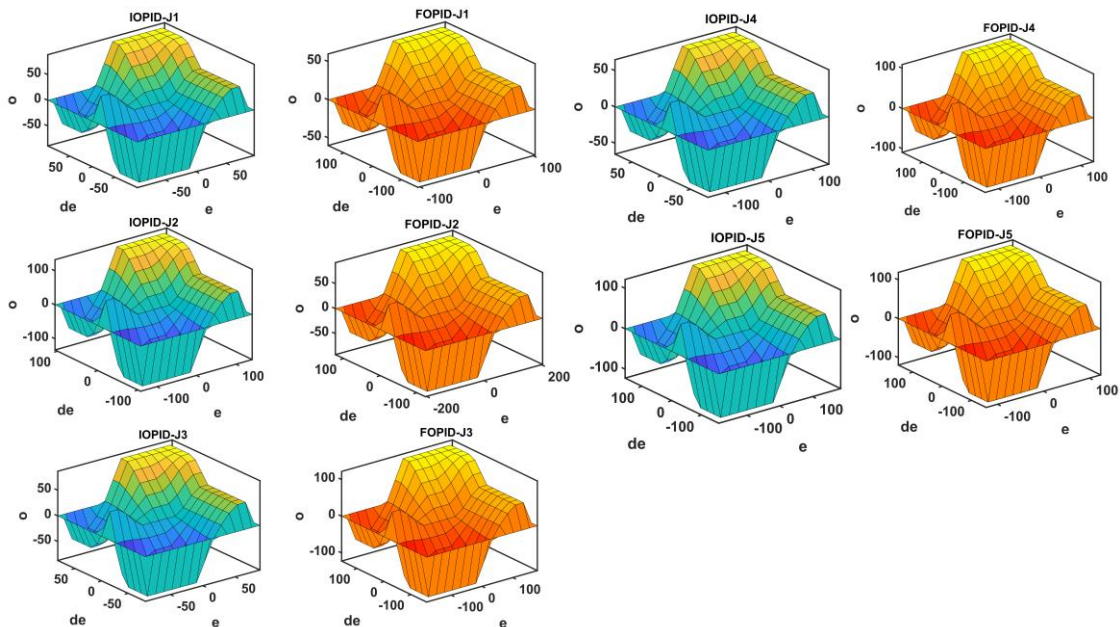
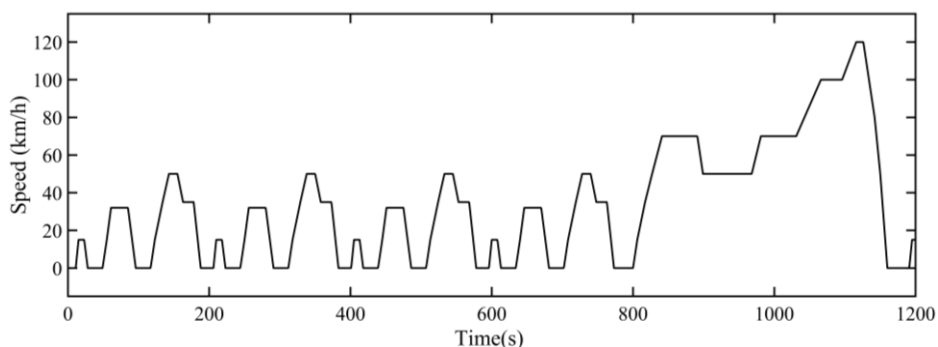


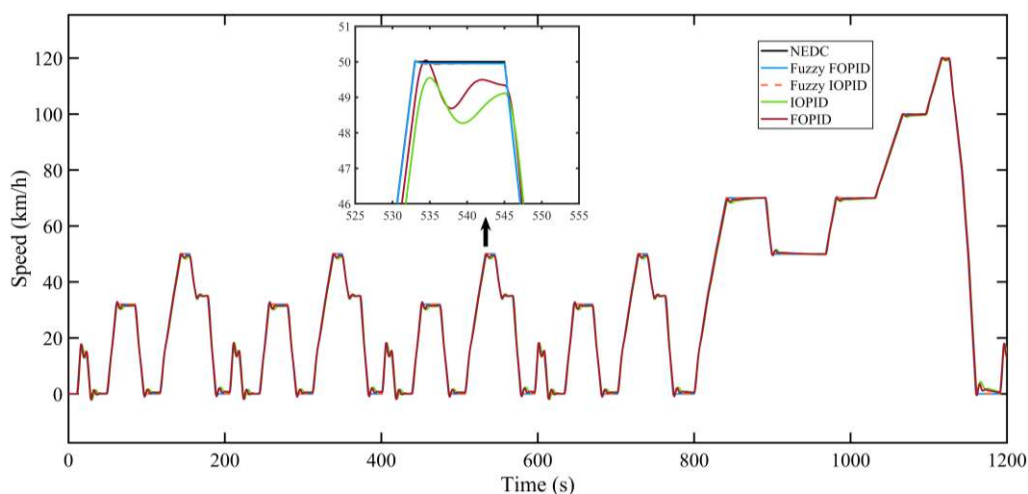
FIGURE 13. Output surface of fuzzy FOPID and IOPID controllers after ACO using  $J_1$ ,  $J_2$ ,  $J_3$ ,  $J_4$ , and  $J_5$  objective functions.



**FIGURE 14.** New European Drive Cycle.

**TABLE IV**  
OPTIMAL SET OF TUNING PARAMETERS FOR FUZZY FOPID AND FUZZY IOPID CONTROLLERS WITH ACO

Controller	Objective function	$K_e$	$K_{de}$	$K_u$	$\lambda$	$\mu$	$X$	$Y$	$Z$
Fuzzy IOPID	$J_1$	46.50	16.98	48.95	1	1	64.51	66.11	89.63
	$J_2$	20.62	13.03	43.91	1	1	94.44	71.02	133.18
	$J_3$	28.72	23.52	29.17	1	1	59.80	55.60	87.83
	$J_4$	46.55	28.62	47.40	1	1	94.44	53.13	65.91
	$J_5$	46.05	39.01	33.76	1	1	124.47	105.05	122.80
Fuzzy FOPID	$J_1$	4.696	28.27	41.45	0.66	0.59	69.81	104.65	60.91
	$J_2$	21.01	38.01	37.02	0.54	0.52	136.68	82.83	92.24
	$J_3$	1.99	45.25	37.91	0.45	0.64	120.87	105.15	52.20
	$J_4$	49.65	41.15	47.70	0.39	0.87	88.13	133.18	109.06
	$J_5$	1.64	33.61	24.17	0.86	0.35	83.83	100.65	119.07



(a)

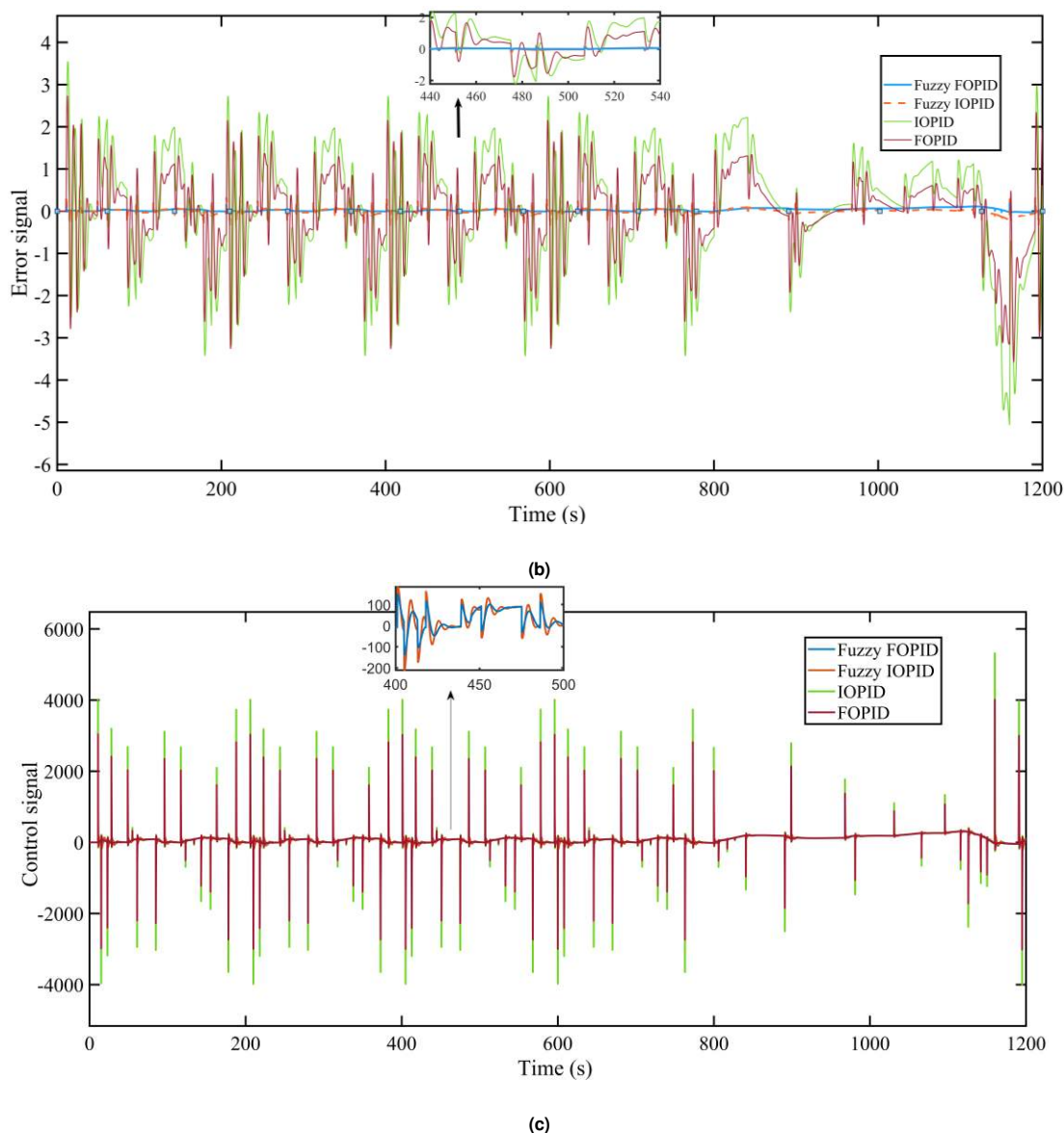


FIGURE 15. Performance of fuzzy FOPID, fuzzy IOPID, FOPID, and IOPID (a) to track NEDC speed test, (b) error signal, (c) controller effort.

TABLE V  
PERFORMANCE PARAMETERS FOR FUZZY FOPID AND IOPID CONTROLLERS

Controller	Objective function	Settling time (sec)	Rise time (sec)	Overshoot (%)	Steady-State error	<i>ITSE</i>	<i>ITAE</i>	<i>IAE</i>	<i>ISE</i>	Total indices
Fuzzy IOPID	$J_1$	1.00	0.595	0.707	0.0008	0.06	9.573	0.626	0.22	10.49
	$J_2$	9.48	1.04	2.28	0.0012	0.20	12.32	1.15	0.390	14.06
	$J_3$	8.51	1.45	2.04	0.0009	0.306	19.39	1.429	0.464	21.59
	$J_4$	3.80	1.66	1.25	0.002	0.318	24.04	1.445	0.451	26.25
	$J_5$	2.02	1.17	0.91	0.0015	0.165	17.06	1.05	0.33	18.61
Fuzzy FOPID	$J_1$	0.83	0.16	0.502	0.0011	0.04	8.83	0.49	0.107	9.46
	$J_2$	1.39	0.14	0.520	0.0018	0.04	10.45	0.465	0.115	11.07
	$J_3$	0.71	0.13	0.510	0.0008	0.22	8.45	0.808	0.228	9.71
	$J_4$	3.35	0.26	0.505	0.0009	0.133	6.028	0.814	0.27	7.25
	$J_5$	<b>0.75</b>	<b>0.081</b>	<b>0.505</b>	<b>0.0001</b>	<b>0.006</b>	<b>5.129</b>	<b>0.192</b>	<b>0.03</b>	<b>5.36</b>

**b. Disturbance Rejection:** The robustness and the effectiveness of the fuzzy FOPID controller are verified in actual working conditions by introducing disturbances. An efficient and robust controller must reject the disturbance such that the deviation from the desired response is minimum. The speed tracking performance of the suggested controllers under the influence of disturbance is shown in Figure 18. The results show that the ACO-based IOPID and the FOPID cannot accurately track the NEDC cycle than the fuzzy-based controllers. The fuzzy-based controllers can return to the set-point value quickly after the appearance of external disturbance. Also, such a system requires less recovery time compared to others.

**c. Noise suppression:**

The EV system's robustness in the presence of measurement noise is tested by introducing a random signal of amplitude -0.04 to +0.04 and sampling time 0.01 seconds. Figure 19 demonstrates the effects of adding the noise input to the system. The fuzzy FOPID gives relatively minor fluctuation than fuzzy IOPID, FOPID, and IOPID controllers, showing a superior and robust control performance in noise suppression.

**d. Sensitivity Analysis and Robustness:** The controllers' robustness is demonstrated by introducing uncertainties and varying EV system parameters. Here, the uncertain parameters of the EV like mass ( $m$ ), drag coefficient ( $C_d$ ), rolling resistance coefficient ( $\mu_{rr}$ ) and EV tire radius ( $r$ ) are varied, and the percentage of variation in these parameters is shown in Table VI. Figure 20 shows the robustness of the suggested controllers against the variations in system parameters, i.e., change in  $m$  by +30%,  $\mu_{rr}$  by +30%,  $C_d$  by -20% and  $r$  by +25%. It is observed that, compared to other controllers, the fuzzy FOPID controller takes the minimum time to complete the full power acceleration and stabilize in the presence of the uncertainties.

TABLE VI  
UNCERTAIN PARAMETERS OF EV SYSTEM

Parameter	Variation %
$R_a + R_f$	+10
$L_a + L_f$	-20
$r$	+25
$J$	-20
$m$	+30
$C_d$	-20
$\mu_{rr}$	+30

The critical frequency domain specifications are [54]:

Sensitivity function

$$S(s) = \frac{1}{1 + L(s)} \quad (26a)$$

Complementary Sensitivity function

$$T(s) = \frac{L(s)}{1 + L(s)} \quad (26b)$$

Disturbance Sensitivity

$$S_d(s) = \frac{G(s)}{1 + L(s)} \quad (26c)$$

Control Sensitivity

$$S_u(s) = \frac{C(s)}{1 + L(s)} \quad (26d)$$

where  $G(s)$  is the plant transfer function,  $C(s)$  indicates the controller transfer function, and  $L(s) = G(s)C(s)$  represents the loop transfer function.

The sensitivity function shows the system's ability to suppress load disturbances and attain good set-point tracking. The complementary sensitivity function specifies the robustness against the measurement noise [54]. The frequency-domain plots of sensitivity function, complementary sensitivity function, disturbance sensitivity, and control sensitivity are shown in Figure 21. For satisfactory system performance, the sensitivity function must have a small value at lower frequencies, and the complementary sensitivity function must have a small value at higher frequencies. The plots show that the fuzzy FOPID controller provides a better load disturbance rejection and a better high-frequency measurement noise rejection than other controllers. It is also observed that the sensitivity peak under fuzzy FOPID controller is minimum, while the conventional IOPID and FOPID controllers have higher sensitivity peaks.

**e. Matignon's theorem and stability analysis:**

**Theorem:** The fractional-order transfer function  $G(s) = N(s)/D(s)$  is stable in  $s$ -plane if and only if the following condition is satisfied [55]:

$$|arg(w_i)| > q \frac{\pi}{2}, \forall w_i \in C, \quad (27)$$

the  $i^{\text{th}}$  root of  $D(w) = 0$ , where  $w = s^q$ , ( $0 < q < 2$ ).

The linearized model of the EV system, which is obtained using system identification, is given by

$$G(s) = \frac{\{ 0.01292s^3 + 0.005944s^2 \}}{\{ +0.0004034s + 1.836e - 05 \}} = \frac{\{ 0.01292s^3 + 0.005944s^2 \}}{\{ +0.01532s^2 + 0.001381s + 4.641e - 05 \}} \quad (28)$$

Here, one set of the ACO based fuzzy controller parameters is considered, i.e.,  $K_u = 23.15$ ,  $K_e = 1.69$ ,  $K_{ce} = 13.78$ ,  $\lambda = 0.514$  and  $\mu = 0.902$ .

Hence, the expression of the FOPID controller takes the form

$$C(s) = 39.12 + \frac{23.15}{s^{0.514}} + 319s^{0.902} \quad (29)$$

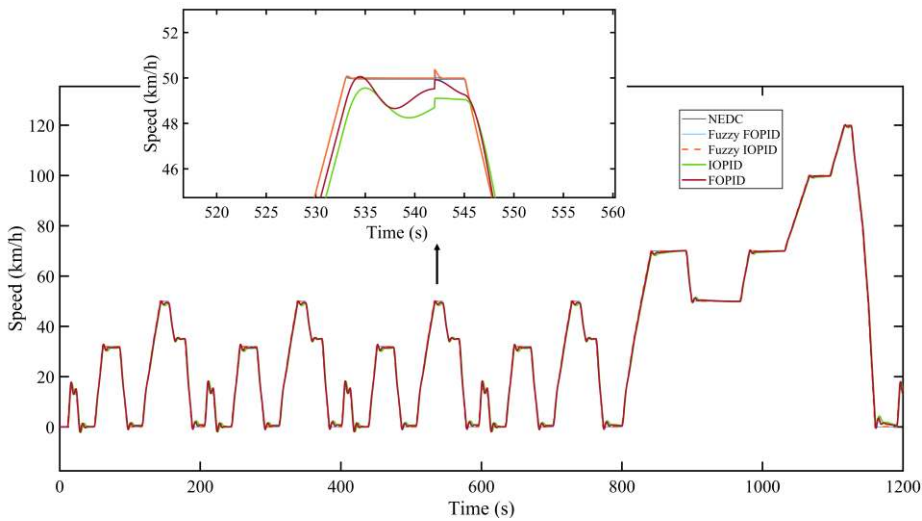


FIGURE 18. Performance of fuzzy FOPID, fuzzy IOPID, FOPID, and IOPID to track NEDC speed test under the influence of disturbance.

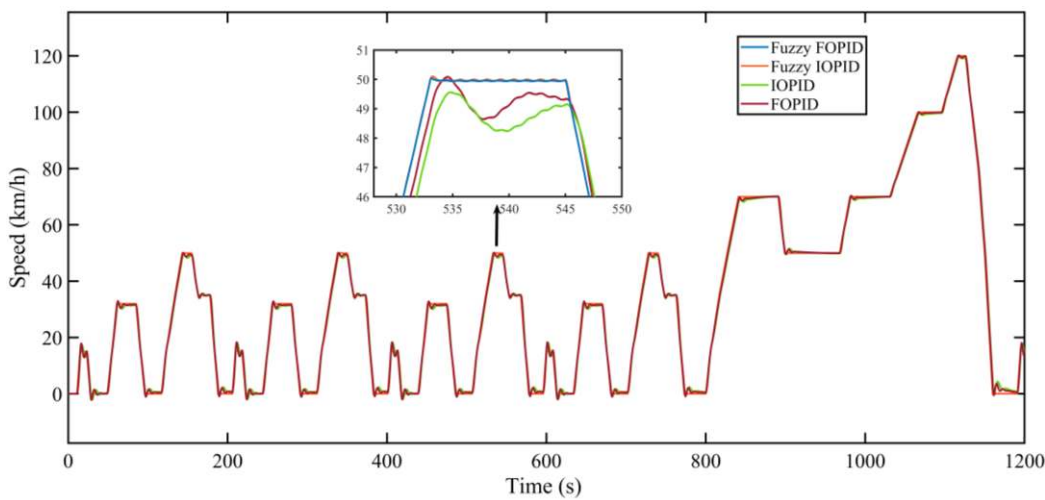


FIGURE 19. Performance of fuzzy FOPID, fuzzy IOPID, FOPID, and IOPID to track NEDC speed test in the presence of measurement noise.

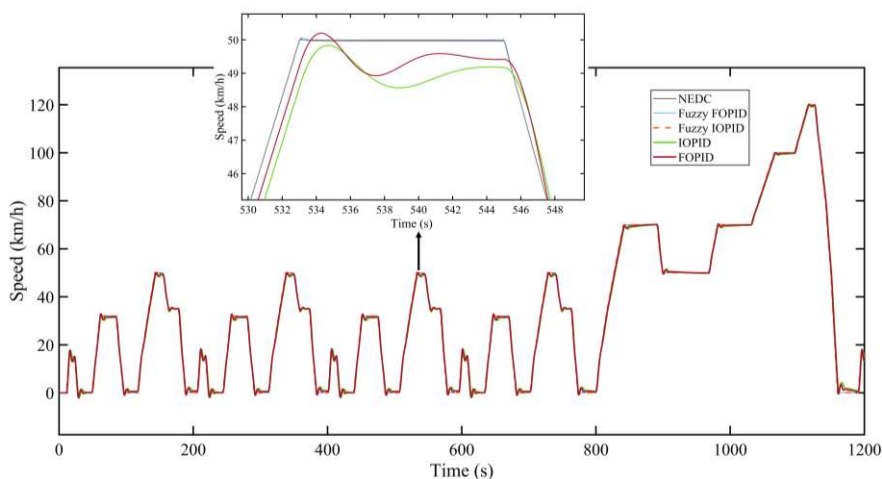


FIGURE 20. Robustness of fuzzy FOPID, fuzzy IOPID, FOPID, and IOPID against the parameter variations of EV, i.e., change in mass by +30%, rolling resistance coefficient by +30%, drag coefficient by -20%, and EV tire radius by +25%.

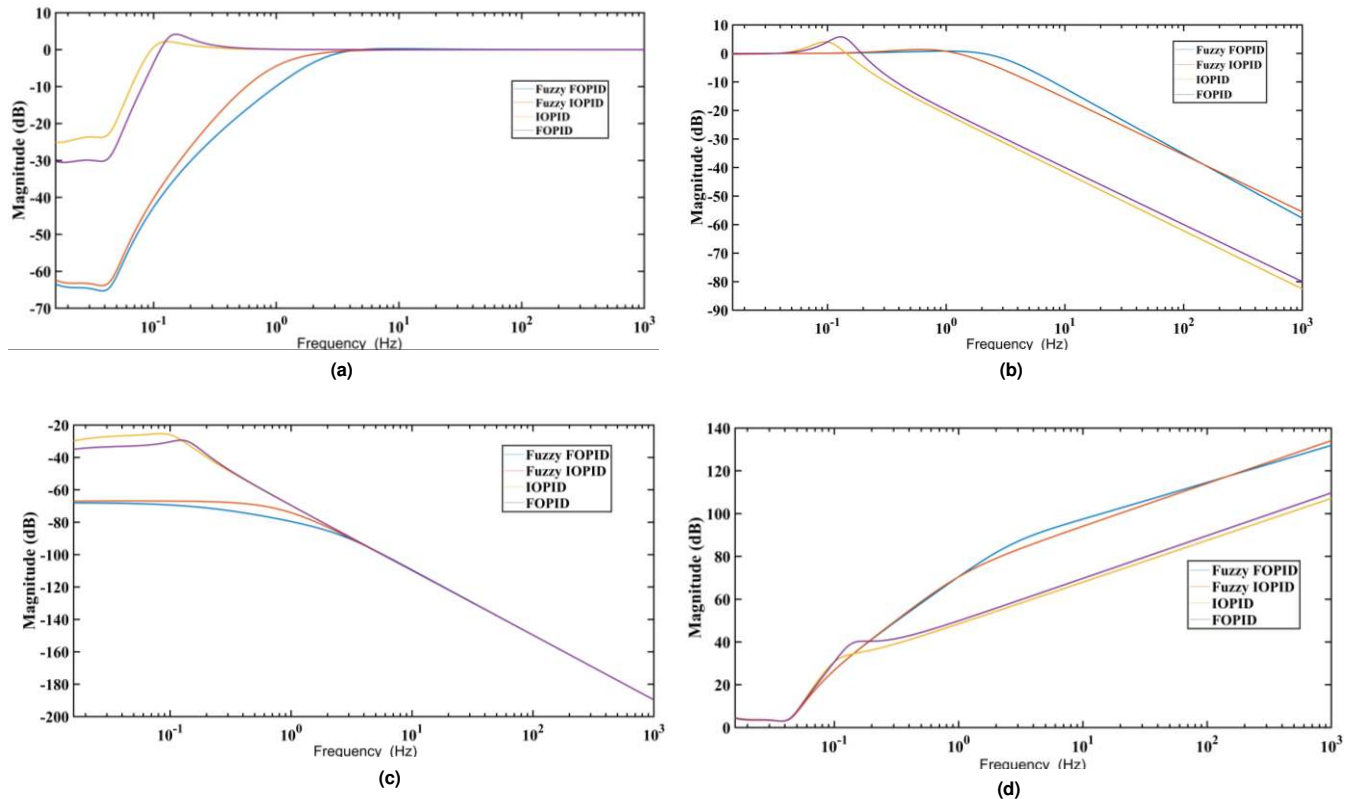


FIGURE 21. Frequency domain plots of (a) Sensitivity function, (b) Complementary sensitivity function, (c) Disturbance sensitivity, and (d) Control sensitivity using fuzzy FOPID, fuzzy IOPID, FOPID, and IOPID controllers.

Hence, the characteristic equation of the system is given as

$$1 + G(s)C(s) = 0$$

$$s^{5.514} + 0.2985s^{4.514} + 4.1151s^{4.416} + 0.61855s^{3.514} + 1.8961s^{3.416} + 0.29863s^3 + 0.24785s^{2.514} + 0.12868s^{2.416} + 0.1376s^2 + 0.017162s^{1.514} + 0.0058568s^{1.416} + 0.0093387s + 0.00076465s^{0.514} + 0.00042503 = 0 \quad (30)$$

This can be rewritten as

$$D(s) = s^{\frac{551.4}{100}} + 0.2985s^{\frac{451.4}{100}} + 4.1151s^{\frac{441.6}{100}} + 0.61855s^{\frac{351.4}{100}} + 1.8961s^{\frac{341.6}{100}} + 0.29863s^{\frac{300}{100}} + 0.24785s^{\frac{251.4}{100}} + 0.12868s^{\frac{241.6}{100}} + 0.1376s^{\frac{200}{100}} + 0.017162s^{\frac{151.4}{100}} + 0.0058568s^{\frac{141.6}{100}} + 0.0093387s^{\frac{100}{100}} + 0.00076465s^{\frac{51.4}{100}} + 0.00042503 = 0 \quad (31)$$

The following transformation is used to map from  $s$ -plane to  $w$ -plane.

$$w = \frac{1}{s^m}, \quad m = 100 \quad (32)$$

Therefore,

$$D(w) = s^{551.4} + 0.2985s^{451.4} + 4.1151s^{441.6} + 0.61855s^{351.4} + 1.8961s^{341.6} + 0.29863s^{300} + 0.24785s^{251.4} + 0.12868s^{241.6} + 0.1376s^{200} + 0.017162s^{151.4} + 0.0058568s^{141.6} + 0.0093387s^{100} + 0.00076465s^{51.4} + 0.00042503 = 0 \quad (33)$$

The stability conditions for the fractional-order system are given as

- The system is stable if

$$\frac{\pi}{2m} < |arg(w)| < \frac{\pi}{m} \quad (34a)$$

- The system is oscillatory if

$$|arg(w)| = \frac{\pi}{2m} \quad (34b)$$

If not, the system is unstable.

The pole-zero plot is obtained by solving (33) using the fractional-order modeling and control (FOMCON) toolbox, as shown in Figure 22. It shows that the system is stable for  $q = 1/m = 0.01$ , and all the poles of  $s^{0.01}$  polynomial are placed in the stable area (outside the red

shaded region), satisfying Matignon's stability theorem [56]. The region of stability depends on the order  $q$ . Since,  $q = 0.01$ , the angle is around  $0.9^\circ$ .

Similarly, during ACO, each combination of controller parameters is subjected to stability check using the Matignon stability theorem. Hence, all the controller parameter values that cause instability of the closed-loop system are rejected.

**f. Eigenvalue Analysis:**

The eigenvalues of the compensated system can be determined using the characteristic equation given by

$$|\lambda I - A_c| = 0 \quad (35)$$

where  $A_c$  is the system matrix of the linearized system with the selected controller,  $\lambda$  is the eigenvalues, and  $I$  is the identity matrix.

**Theorem:** If all the eigenvalues of  $A_c$  satisfy the condition

$$|\arg(\lambda(A_c))| > \frac{q\pi}{2} \quad (36)$$

then the zero solution of the system is asymptotically stable. The proof of this theorem is detailed in [56].

There are 551 roots, and all roots of the characteristic equation satisfy the (36) and lie within the stable region, as shown in Figure 22. This condition assures that the system is bounded input bounded output (BIBO) stable and asymptotically stable.

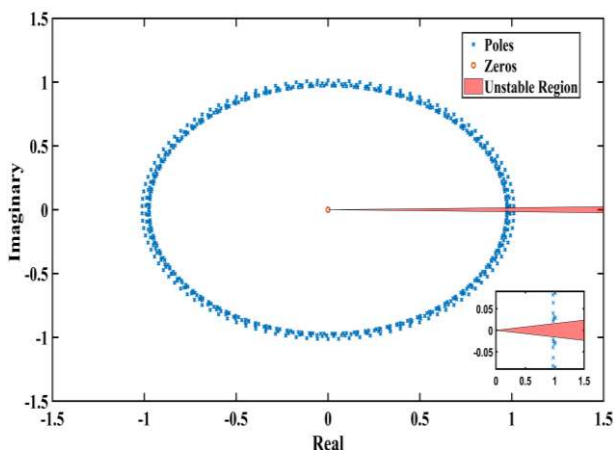


FIGURE 22. Stability plot for the closed-loop EV system.

**g. Comparison of ACO based fuzzy FOPID controller with other optimization algorithms and existing controllers:**

The ACO-based fuzzy FOPID controller's speed tracking performance is compared with the GA-based fuzzy FOPID controller and the PSO-based fuzzy FOPID controller. The parameters considered for the PSO are the

maximum iteration = 100, population size = 100, acceleration factors  $c_1 = c_2 = 2$  and inertia weights  $w_{max} = 0.9$  and  $w_{min} = 0.4$ . Similarly, the parameters of the GA optimization are also selected. Here, maximum generation is taken as 100, population size = 100, crossover fraction = 0.8 and mutation fraction = 0.2. In all the cases,  $J_5$  is considered as the objective function to be minimized. Here, the lower and upper bounds of the controller parameters and adjustable membership parameters are taken from Table III. Table VII gives the EV time-domain performance and the performance indices using the above-considered controllers. It is evident from the results that the ACO-based fuzzy FOPID controller is better than the other controllers. Also, the PSO-based fuzzy FOPID controller gives better performance than the GA-based controller.

Three standard error measurement criteria that can evaluate the efficiency of the proposed controller with other existing controllers are the sum of squared errors (SSE), mean absolute error (MAE), and mean square error (MSE). Table VIII shows the performance comparison of the proposed controller to multi-objective PI [30], multi-objective fuzzy PI [30], and model predictive control (MPC) [4] controllers. It is observed that the proposed controller yields an optimal performance as the values of their error measurement criteria are close to zero.

Despite the various merits of the schemes discussed, it has a couple of limitations: (i) Framing the fuzzy rule base for the fuzzy logic controller to track the new European drive cycle (NEDC) test is time-consuming as it requires expertise and experience. (ii) More number of parameters (eight parameters) are used in optimization.

**A. CIRCUIT REALIZATION OF FOPID CONTROLLER**

The EX-CCII based FOPID controller circuit in Figure 8 is simulated in the Cadence analog design environment using a 180 nm GPDK CMOS process. Table IX shows the design details and aspect ratios ( $W/L$ ) for MOS transistors used in Figure 10.

In the CMOS circuit of three input EX-CCII, all transistors operate in the saturation region, and DC bias current  $I_0$  is distributed using the NMOS and the PMOS current mirrors with the aspect ratios  $5 \mu\text{m}/1 \mu\text{m}$  and  $25 \mu\text{m}/5 \mu\text{m}$ , respectively. Similarly, the DC bias current  $I_B$  in the summation stage is distributed using the NMOS and PMOS current mirrors with aspect ratios  $2.5 \mu\text{m}/1 \mu\text{m}$  and  $24 \mu\text{m}/10 \mu\text{m}$ , respectively.

The fuzzy FOPID controller parameters in (29) are used to evaluate the performance of the FOPID controller circuit in Figure 8. Using Eq. (22) and (29), the circuit parameters are calculated as  $R_1 = 1 \text{ k}\Omega$ ,  $R_2 = 39.12 \text{ k}\Omega$ ,  $R_\lambda = 4.319 \text{ k}\Omega$ ,  $C_\lambda = 10 \mu\text{sec}^{0.486}$ ,  $R_\mu = 31.19 \text{ M}\Omega$  and  $C_\mu = 10 \mu\text{sec}^{0.0908}$ .



TABLE VII  
COMPARISON OF PERFORMANCE OF ACO, PSO, AND GA BASED FUZZY FOPID CONTROLLER FOR EV SPEED CONTROL

Controller	Objective function	Settling time (sec)	Rise time (sec)	Overshoot (%)	Steady-state error	ITSE	ITAE	IAE	ISE	Total indices
Fuzzy FOPID ACO	$J_5$	<b>0.75</b>	<b>0.081</b>	<b>0.505</b>	<b>0.0009</b>	<b>0.006</b>	<b>5.129</b>	<b>0.192</b>	<b>0.03</b>	<b>5.36</b>
Fuzzy FOPID GA	$J_5$	1.4	0.19	0.80	0.0021	0.040	6.12	0.412	0.23	6.80
Fuzzy FOPID PSO	$J_5$	1.2	0.12	0.72	0.0010	0.020	5.75	0.311	0.11	6.20

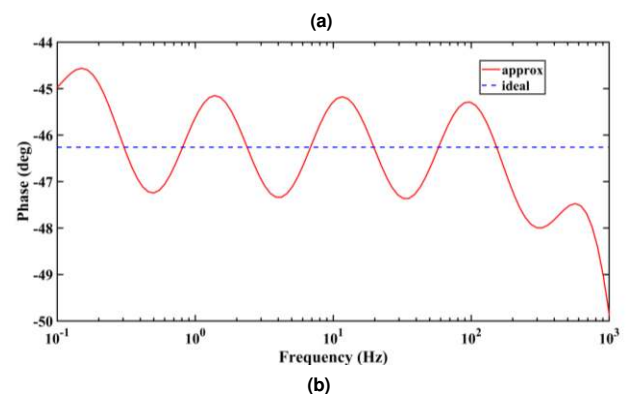
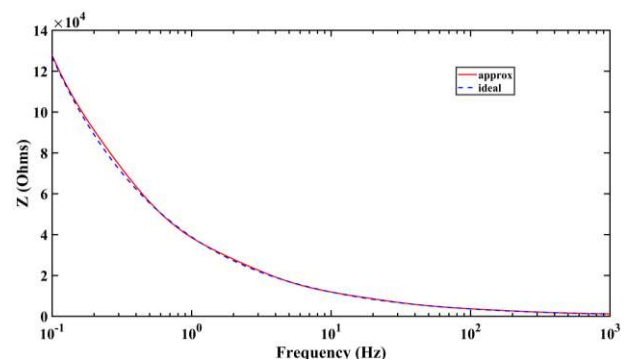
TABLE VIII  
COMPARISON OF PERFORMANCE OF ACO BASED FUZZY CONTROLLER WITH OTHER EXISTING CONTROLLERS

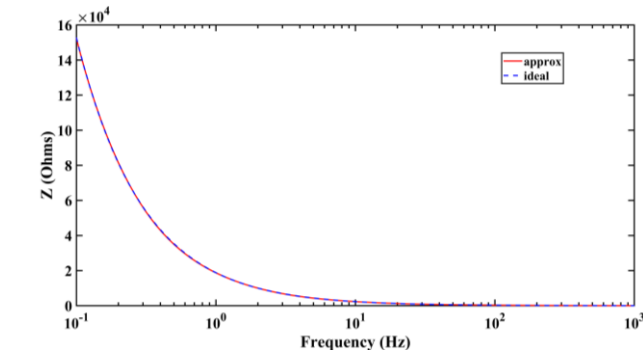
Criteria	ACO Fuzzy FOPID [This work]	PI [44]	Fuzzy PI [44]	MPC [4]
SSE	<b>2.711</b>	14.021	10.600	7.090
MAE	<b>0.005</b>	0.101	0.0984	0.010
MSE	<b><math>6.100 \times 10^{-5}</math></b>	$9.919 \times 10^{-4}$	$4.697 \times 10^{-4}$	$1.990 \times 10^{-4}$

TABLE IX  
DESIGN DETAILS FOR THREE INPUT EX-CCII AND THREE INPUT SUMMATION CIRCUITS

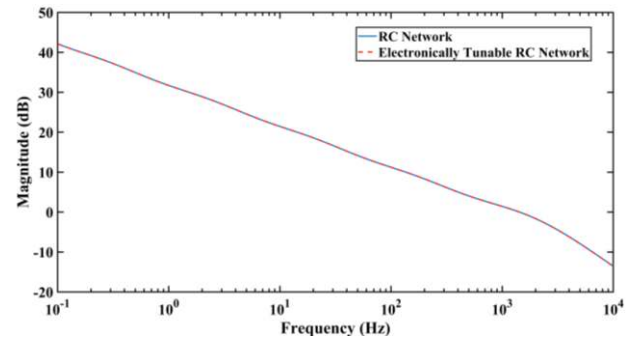
Process	180 nm GPDK CMOS	
Supply voltage	$V_{DD} = -V_{SS}$	0.9 V
Three input EX-CCII circuit in Fig. 10 (a)	$I_0$	12 $\mu$ A
	$\left(\frac{W}{L}\right)_{Mn1-Mn4}$	$\frac{25 \mu\text{m}}{2 \mu\text{m}}$
	$\left(\frac{W}{L}\right)_{Mn5-Mn10}$	$\frac{1 \mu\text{m}}{5 \mu\text{m}}$
	$I_B$	10 $\mu$ A
	$R$	5.8 k $\Omega$
Three input summation circuit in Fig. 10 (b)	$\left(\frac{W}{L}\right)_{Mn1a-Mn6a}$	$\frac{20 \mu\text{m}}{2 \mu\text{m}}$
	$\left(\frac{W}{L}\right)_{Mp1a-Mp2a}$	$\frac{25 \mu\text{m}}{1 \mu\text{m}}$

The fractional-order capacitors used in the fractional-order differentiator and the integrator stages are approximated using the 5<sup>th</sup> order modified Oustaloup method and realized using the Valsa RC networks, given in Figure 9, to cover the frequency range [0.1 Hz, 1000 Hz] with the phase accuracy of 1°. The behaviour of the Valsa RC network used to implement the constant phase element is verified by plotting the impedance frequency response, along with the ideal response, as shown in Figure 23. The resistors in a Valsa RC network are realized using the CMOS circuits of electronically tunable OTA simulated resistors in Figure 12, and their values are tuned by adjusting the bias current.

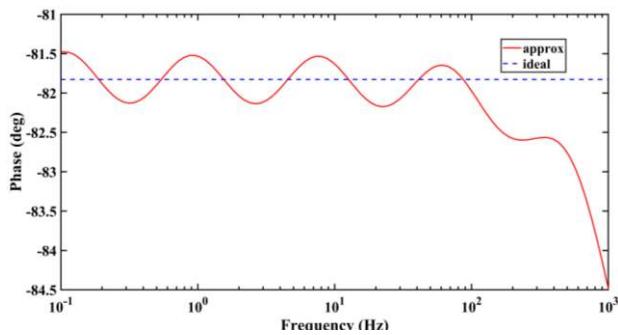




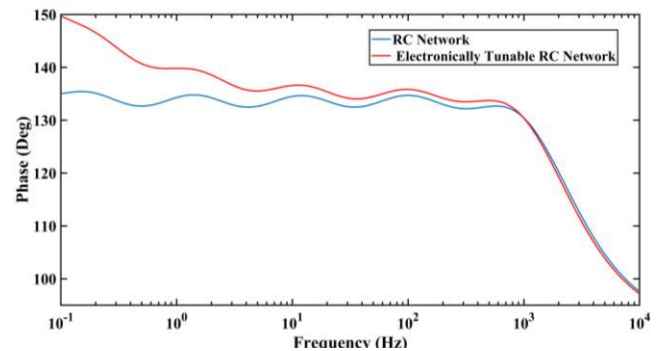
(c)



(a)



(d)



(b)

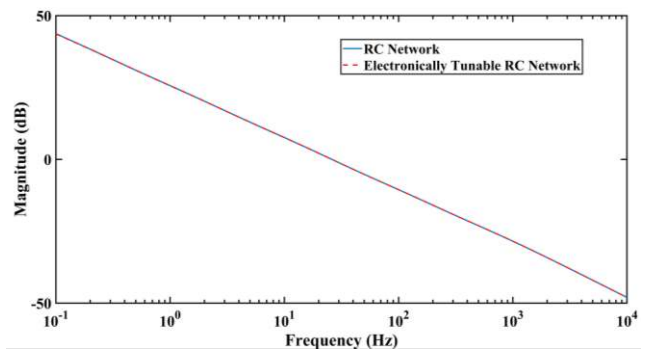
**FIGURE 23.** Impedance frequency response of Valsa RC networks approximating the fractional-order capacitors:  $C_\lambda=10 \mu/\text{sec}^{0.486}$  (a) magnitude (b) phase and  $C_\mu = 10 \mu/\text{sec}^{0.0908}$  (c) magnitude, (d) phase.

Here, the  $R = 1/g_m$ , where  $g_m$  is the transconductance of the differential MOS pair in Figure 12, and the values of DC bias currents are calculated using (25a)-(25b). Also, the aspect ratios of the MOS transistors Mp1b-Mp4b are set as  $25 \mu\text{m}/2 \mu\text{m}$  and Mn1b-Mn4b as  $10 \mu\text{m}/2 \mu\text{m}$ . Table X summarizes the value of resistors, dc bias currents, and capacitors used in the Valsa RC network.

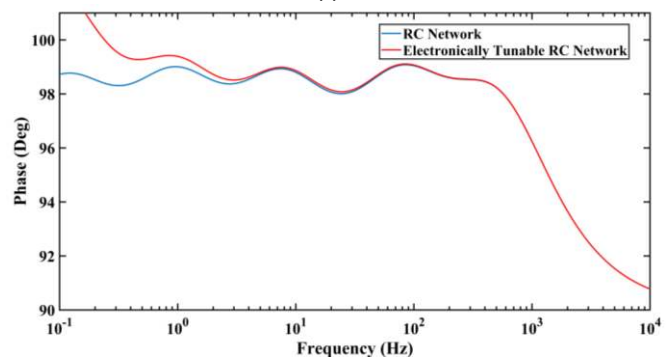
TABLE X

VALUES OF RESISTORS, DC BIAS CURRENTS, AND CAPACITORS OF VALSA RC NETWORKS USED TO REALIZE FRACTIONAL-ORDER CAPACITORS

Element	$C_\lambda=10 \mu/\text{sec}^{0.486}$	$C_\mu = 10 \mu/\text{sec}^{0.0908}$
$R_p (I_p)$	374.74 k $\Omega$ (210 nA)	4.27 M $\Omega$ (16 nA)
$R_1 (I_1)$	189.86 k $\Omega$ (450 nA)	740.4 k $\Omega$ (100 nA)
$R_2 (I_2)$	63.84 k $\Omega$ (1.5 $\mu\text{A}$ )	109.3 k $\Omega$ (830 nA)
$R_3 (I_3)$	21.47 k $\Omega$ (5 $\mu\text{A}$ )	16.15 k $\Omega$ (7 $\mu\text{A}$ )
$R_4 (I_4)$	7.22 k $\Omega$ (19 $\mu\text{A}$ )	2.38 k $\Omega$ (160 $\mu\text{A}$ )
$R_5 (I_5)$	2.42 k $\Omega$ (100 $\mu\text{A}$ )	1 k $\Omega$ (330 $\mu\text{A}$ )
$C_p$	75.41 $\mu\text{F}$	4.05 $\mu\text{F}$
$C_1$	8.38 $\mu\text{F}$	2.15 $\mu\text{F}$
$C_2$	2.99 $\mu\text{F}$	1.74 $\mu\text{F}$
$C_3$	1.06 $\mu\text{F}$	1.41 $\mu\text{F}$
$C_4$	380.90 nF	1.15 $\mu\text{F}$
$C_5$	135.92 nF	936 nF



(c)



(d)

**FIGURE 24.** Frequency response of Valsa RC networks using passive resistors and electronically tunable resistors used to realize the fractional-order capacitors:  $C_\lambda=10 \mu/\text{sec}^{0.486}$  (a) magnitude, (b) phase and  $C_\mu = 10 \mu/\text{sec}^{0.0908}$  (c) magnitude, (d) phase.

TABLE XI  
COMPARISON OF THE PROPOSED CONTROLLER SCHEME WITH OTHER EXISTING SOLUTIONS

Factors	This work	[32]	[33]	[57]	[35]	[34]
Technology	<b>CMOS (GPDK 180 nm)</b>	CMOS (AMS 0.35 $\mu\text{m}$ )	CMOS (AMS 0.35 $\mu\text{m}$ )	---	CMOS ON (0.7 $\mu\text{m}$ )	CMOS (AMS 0.35 $\mu\text{m}$ )
No. of active blocks	<b>1 EX-CCII +14 OTAs</b>	29 OTAs	16 OTAs	20 CFOAs	4 VDCCs	1 EX-CCII
No. of resistors and capacitors	<b>12C</b>	10C	6C	44R +10C	10R+8C	14R+12C
All grounded capacitors	<b>Yes</b>	Yes	Yes	Yes	Yes	Yes
Electronic tuning	<b>Yes</b>	Yes	Yes	No	Yes	No

R - Resistor, C - Capacitor, OTA - Operational transconductance amplifier, EX-CCII - Extra input CCII, CFOA - Current feedback operational amplifier, VDCC – Voltage differencing current conveyor

Figure 24 presents the magnitude and phase responses of the Valsa RC networks using the passive resistors and the electronically tunable resistors. It shows that the magnitude response error is negligible, and the error in the phase plot is about 10%. These errors are caused due to the OTA's imperfections. The gain and phase responses of EX-CCII based FOPID controller circuits are depicted in Figure 25, which confirm the controller's accurate operation. Any set of the controller parameters of the fuzzy FOPID controller can be realized using the circuit, shown in Figure 8, by electronically tuning the OTA simulated resistors.

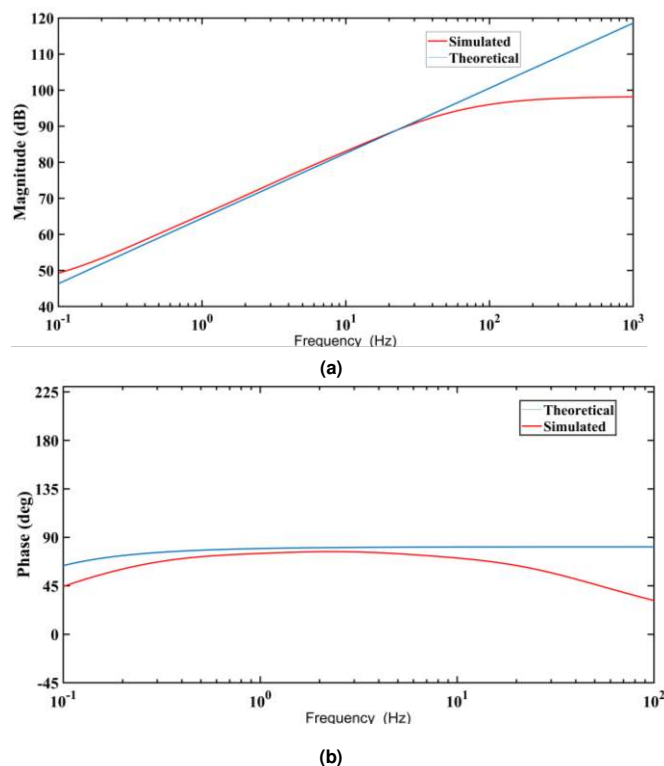


FIGURE 25. Frequency response of the designed controller (a) magnitude, (b) phase.

Table XI shows the comparison of the critical features of the proposed FOPID circuit to other previously reported solutions

based on various active elements. Based on Table XI, it is evident that in the proposed scheme, there is a significant reduction in active element count and passive resistors. OTA-based simulated resistors replace the passive resistors in the controller circuit and offer electronic tunability.

## VI. CONCLUSION

This study presents a novel approach in designing and developing a multi-objective fuzzy FOPID for speed control of EV. The EV can be controlled in real-time by adjusting the control parameters and the membership functions via ACO when the system encounters disturbance, parameter uncertainties, and varying road conditions. The fuzzy fractional-order controllers have become industrial control standards due to their improved robustness against plant parameter variations and system perturbation, and better disturbance rejection control. The controller's significant advantage is its ability to reduce control effort, reducing the energy wasted in various industrial control applications. The proposed controller can be effectively employed for EV speed tracking. The effectiveness and the robustness of the proposed novel controller have been comprehensively illustrated by subjecting it to disturbance and uncertainties. The significant outcomes of this investigation are summarized as:

1. The performance of ACO-based fuzzy FOPID was compared with the fuzzy IOPID, FOPID, and classical IOPID, and it was observed that the proposed controller gave the fastest tracking response with a settling time of 0.75 sec and a rise time of 0.081 sec. The controller exhibited a small overshoot of 0.5% and a steady-state error of 0.0001. Furthermore, the proposed controller gives a remarkable reduction in error indices, such as *IAE*, *ISE*, *ITAE*, and *ITSE*, by 87%, 93%, 78%, and 98%, respectively, when compared with other controllers.
2. The simulation results also revealed that the proposed controller could excellently handle parameter variation, uncertainties, disturbance, and noise compared to the other controllers. The proposed controller's robustness was tested under the following EV parameter variations

- from its nominal value, i.e., change in mass +30%, change in rolling resistance +30%, change in drag coefficient -20%, and change in EV tire radius +25%.
- The stability of the system is also investigated using Matignon's stability theorem and eigenvalue analysis.
  - The ACO-based fuzzy FOPID controller's speed tracking performance was evaluated and compared with the PSO and the GA optimized fuzzy FOPID controllers. It was found that the ACO-based controller gave a faster convergence and low values of performance indices, i.e.,  $ITSE = 0.006$ ,  $ITAE = 5.129$ ,  $IAE = 0.192$ ,  $ISE = 0.03$ , and the sum of indices was 5.36.
  - The proposed controller was realized using a single EX-CCII block that offered design flexibility and electronic tunability. It also allowed the simultaneous realization of the fractional-order integrator and differentiator stages of different orders. This circuit can be used to realize any combination of the fuzzy FOPID controller parameters by adjusting the bias currents in OTA-based resistors. The proposed circuit uses a minimum number of passive elements that make it energy effective. The controller can be implemented using the integrated circuits of analog blocks, and its performance can be verified in real-time.

This investigation expects to give valuable insights for future simulation studies that can be validated using the real-time experimental setup to control EVs' speed. The proposed fuzzy FOPID controller is well suited for cruise control applications in EV and can also be used in EV battery recharging or discharging applications under constant DC voltage. As a future scope, the fuzzy-based controller can be extended to an Adaptive Neuro-Fuzzy Inference System (ANFIS), which combines the advantages of fuzzy inference systems and neural networks. It provides better learning and adaptation capability without requiring expert knowledge.

## REFERENCES

- M. Veysi, J. Aghaei, M. Shasadeghi, R. Razzaghi, B. Bahrani, and D. J. Ryan, "Energy-efficient Speed Control of Electric Vehicles: Linear Matrix Inequality Approach," *IEEE Trans. Veh. Technol.*, vol. 69, no. 10, pp. 10469-10483, July 2020, doi: 10.1109/tvt.2020.3008500.
- M. S. Kumar and S. T. Revankar, "Development scheme and key technology of an electric vehicle: An overview," *Renew. Sustain. Energy Rev.*, vol. 70, pp. 1266-1285, Apr. 2017, doi: 10.1016/j.rser.2016.12.027.
- W. J. Lee, G. Strbac, Z. Hu, Z. Ding, P. Sarikprueck, F. Teng, and G. Kariniotakis, "Special Issue on Advanced Approaches and Applications for Electric Vehicle Charging Demand Management," *IEEE Trans. Ind. Appl.*, vol. 56, no. 5, pp. 5682-5683, Sept. 2020, doi: 10.1109/tia.2020.3003567.
- M. H. Khooban, N. Vafamand, and T. Niknam, "T-S fuzzy model predictive speed control of electrical vehicles," *ISA Trans.*, vol. 64, pp. 231-240, Sept. 2016, doi: 10.1016/j.isatra.2016.04.019.
- M. H. Khooban, T. Niknam, F. Blaabjerg, and M. Dehghani, "Free chattering hybrid sliding mode control for a class of non-linear systems: Electric vehicles as a case study," *IET Sci. Meas. Technol.*, vol. 10, no. 7, pp. 776-785, Oct. 2016, doi: 10.1049/iet-smt.2016.0091.
- K. J. Åström and T. Hägglund, "The future of PID control," *Control Eng. Pract.*, vol. 9, no. 11, pp. 1163-1175, Nov. 2001, doi: 10.1016/S0967-0661(01)00062-4.
- K. H. Ang, G. Chong, and Y. Li, "PID control system analysis, design, and technology," *IEEE Trans. Control Syst. Technol.*, vol. 13, no. 4, pp. 559-576, June 2005, doi: 10.1109/TCST.2005.847331.
- Y. Arya, "Impact of ultra-capacitor on automatic generation control of electric energy systems using an optimal FFOID controller," *Int. J. Energy Res.*, vol. 43, no. 14, pp. 8765-8778, Nov. 2019, doi: 10.1002/er.4767.
- K. Premkumar and B. V. Manikandan, "Bat algorithm optimized fuzzy PD based speed controller for brushless direct current motor," *Eng. Sci. Technol. an Int. J.*, vol. 19, no. 2, pp. 818-840, June 2016, doi: 10.1016/j.jestech.2015.11.004.
- M. Rabah, A. Rohan, Y. J. Han, and S. H. Kim, "Design of fuzzy-PID controller for quadcopter trajectory-tracking," *Int. J. Fuzzy Log. Intell. Syst.*, vol. 18, no. 3, pp. 204-213, Sept. 2018, doi: 10.5391/IJFIS.2018.18.3.204.
- B. E. Demir, R. Bayir, and F. Duran, "Real-time trajectory tracking of an unmanned aerial vehicle using a self-tuning fuzzy proportional integral derivative controller," *Int. J. Micro Air Veh.*, vol. 8, no. 4, pp. 252-268, Dec. 2016, doi: 10.1177/1756829316675882.
- Y. Tao *et al.*, "Fuzzy PID control method of deburring industrial robots," *J. Intell. Fuzzy Syst.*, vol. 29, no. 6, pp. 2447-2455, Jan. 2015, doi: 10.3233/IFS-151945.
- Y. Arya, "AGC performance enrichment of multi-source hydrothermal gas power systems using new optimized FOPID controller and redox flow batteries," *Energy*, vol. 127, pp. 704-715, May 2017, doi: 10.1016/j.energy.2017.03.129.
- P. Khatun, C. M. Bingham, N. Schofield, and P. H. Mellor, "Application of Fuzzy Control Algorithms for Electric Vehicle Antilock Braking/Traction Control Systems," *IEEE Trans. Veh. Technol.*, vol. 52, no. 5, pp. 1356-1364, Sept. 2003, doi: 10.1109/TVT.2003.815922.
- S. Poorani, K. Udaya Kumar, and S. Renganarayanan, "Intelligent controller design for electric vehicle," *IEEE Veh. Technol. Conf.*, vol. 4, pp. 2447-2450, Apr. 2003, doi: 10.1109/vetecs.2003.1208830.
- C. A. Monje, B. M. Vinagre, V. Feliu, and Y. Q. Chen, "Tuning and auto-tuning of fractional order controllers for industry applications," *Control Eng. Pract.*, vol. 16, no. 7, pp. 798-812, July 2008, doi: 10.1016/j.conengprac.2007.08.006.
- F. Padula and A. Visioli, "Tuning rules for optimal PID and fractional-order PID controllers," *J. Process Control*, vol. 21, no. 1, pp. 69-81, Jan. 2011, doi: 10.1016/j.jprocont.2010.10.006.
- A. Tepljakov, E. A. Gonzalez, E. Petlenkov, J. Belikov, C. A. Monje, and I. Petráš, "Incorporation of fractional-order dynamics into an existing PI/PID DC motor control loop," *ISA Trans.*, vol. 60, pp. 262-273, Jan. 2016, doi: 10.1016/j.isatra.2015.11.012.
- D. Guha, P. K. Roy, S. Banerjee, S. Padmanaban, F. Blaabjerg, and D. Chittathuru, "Small-Signal Stability Analysis of Hybrid Power System with Quasi-Opportunistic Sine Cosine Algorithm Optimized Fractional Order PID Controller," *IEEE Access*, vol. 8, pp. 155971-155986, Aug. 2020, doi: 10.1109/ACCESS.2020.3018620.
- H. Kuttomparambil Abdulkhader, J. Jacob, and A. T. Mathew, "Robust type-2 fuzzy fractional order PID controller for dynamic stability enhancement of power system having RES based microgrid penetration," *Int. J. Electr. Power Energy Syst.*, vol. 110, pp. 357-371, Sept. 2019, doi: 10.1016/j.ijepes.2019.03.027.
- M. A. Hannan, J. A. Ali, M. H. Lipu, A. Mohamed, P. J. Ker, T. I. Mahlia, M. Mansor, A. Hussain, K. M. Muttaqi, and Z. Y. Dong, "Role of optimization algorithms based fuzzy controller in achieving induction motor performance enhancement," *Nat. Commun.*, vol. 11, no. 1, pp. 1-11, July 2020, doi: 10.1038/s41467-020-17623-5.
- S. Çeven, A. Albayrak, and R. Bayir, "Real-time range estimation in electric vehicles using fuzzy logic classifier," *Comput. Electr. Eng.*, vol. 83, pp. 106577, May. 2020, doi: 10.1016/j.compeleceng.2020.106577.

- [23] A. Rubaai, M. J. Castro-Sitiriche, and A. R. Ofofi, "DSP-Based laboratory implementation of hybrid fuzzy-PID controller using genetic optimization for high-performance motor drives," *IEEE Trans. Ind. Appl.*, vol. 44, no. 6, pp. 1977-1986, Nov. 2008, doi: 10.1109/TIA.2008.2006347.
- [24] I. Pan, S. Das, and A. Gupta, "Tuning of an optimal fuzzy PID controller with stochastic algorithms for networked control systems with random time delay," *ISA Trans.*, vol. 50, no. 1, pp. 28-36, Jan. 2011, doi: 10.1016/j.isatra.2010.10.005.
- [25] J. A. Ali, M. A. Hannan, A. Mohamed, and M. G. M. Abdolrasol, "Fuzzy logic speed controller optimization approach for induction motor drive using backtracking search algorithm," *Meas. J. Int. Meas. Confed.*, vol. 78, pp. 49-62, Jan. 2016, doi: 10.1016/j.measurement.2015.09.038.
- [26] O. Castillo, F. Valdez, J. Soria, L. Amador-Angulo, P. Ochoa, and C. Peraza, "Comparative study in fuzzy controller optimization using bee colony, differential evolution, and harmony search algorithms," *Algorithms*, vol. 12, no. 1, pp. 1-21, Jan. 2019, doi: 10.3390/a12010009.
- [27] S. Das, I. Pan, S. Das, and A. Gupta, "A novel fractional order fuzzy PID controller and its optimal time domain tuning based on integral performance indices," *Eng. Appl. Artif. Intell.*, vol. 25, no. 2, pp. 430-442, Mar. 2012, doi: 10.1016/j.engappai.2011.10.004.
- [28] V. Kumar, K. P. S. Rana, and P. Mishra, "Robust speed control of hybrid electric vehicle using fractional order fuzzy PD and PI controllers in cascade control loop," *J. Franklin Inst.*, vol. 353, no. 8, pp. 1713-1741, May 2016, doi: 10.1016/j.jfranklin.2016.02.018.
- [29] A. Zamani, S. M. Barakati, and S. Yousofi-Darmian, "Design of a fractional order PID controller using GBMO algorithm for load-frequency control with governor saturation consideration," *ISA Trans.*, vol. 64, pp. 56-66, Sept. 2016, doi: 10.1016/j.isatra.2016.04.021.
- [30] M. Al-Dhaifallah, N. Kanagaraj, and K. S. Nisar, "Fuzzy Fractional-Order PID Controller for Fractional Model of Pneumatic Pressure System," *Math. Probl. Eng.*, vol. 2018, Article ID 5478781, 9 pages, Jan. 2018, doi: 10.1155/2018/5478781.
- [31] X. Wu, Y. Xu, J. Liu, C. Lv, J. Zhou, and Q. Zhang, "Characteristics analysis and fuzzy fractional-order PID parameter optimization for primary frequency modulation of a pumped storage unit based on a multi-objective gravitational search algorithm," *Energies*, vol. 13, no. 1, pp. 137, Jan. 2019, doi: 10.3390/en13010137.
- [32] I. Dimeas, I. Petras, and C. Psychalinos, "New analog implementation technique for fractional-order controller: A DC motor control," *AEU - Int. J. Electron. Commun.*, vol. 78, pp. 192-200, Aug. 2017, doi: 10.1016/j.aeue.2017.03.010.
- [33] S. Kapoulea, V. Bizonis, P. Bertsiyas, C. Psychalinos, A. Elwakil, and I. Petráš, "Reduced active components count electronically adjustable fractional-order controllers: Two design examples," *Electron.*, vol. 9, no. 1, pp. 63, Jan. 2020, doi: 10.3390/electronics9010063.
- [34] S. Kapoulea, C. Psychalinos, and A. S. Elwakil, "Single active element implementation of fractional-order differentiators and integrators," *AEU - Int. J. Electron. Commun.*, vol. 97, pp. 6-15, Dec. 2018, doi: 10.1016/j.aeue.2018.09.046.
- [35] O. Domansky, R. Sotner, L. Langhammer, J. Jerabek, C. Psychalinos, and G. Tsimokou, "Practical Design of RC Approximants of Constant Phase Elements and Their Implementation in Fractional-Order PID Regulators Using CMOS Voltage Differencing Current Conveyors," *Circuits, Syst. Signal Process.*, vol. 38, no. 4, pp. 1520-1546, Apr. 2019, doi: 10.1007/s00034-018-0944-z.
- [36] R. Sharma, K. P. S. Rana, and V. Kumar, "Performance analysis of fractional order fuzzy PID controllers applied to a robotic manipulator," *Expert Syst. Appl.*, vol. 41, no. 9, pp. 4274-4289, July 2014, doi: 10.1016/j.eswa.2013.12.030.
- [37] C. S. Shieh, "Fuzzy PWM based on Genetic Algorithm for battery charging," *Appl. Soft Comput. J.*, vol. 21, pp. 607-616, Aug. 2014, doi: 10.1016/j.asoc.2014.04.009.
- [38] A. Mughees and S. A. Mohsin, "Design and Control of Magnetic Levitation System by Optimizing Fractional Order PID Controller Using Ant Colony Optimization Algorithm," *IEEE Access*, vol. 8, pp. 116704-116723, June 2020, doi: 10.1109/ACCESS.2020.3004025.
- [39] M. Birattari, P. Pellegrini, and M. Dorigo, "On the invariance of ant colony optimization," *IEEE Trans. Evol. Comput.*, vol. 11, no. 6, pp. 732-742, Nov. 2007, doi: 10.1109/TEVC.2007.892762.
- [40] M. Wang, T. Ma, G. Li, X. Zhai, and S. Qiao, "Ant Colony Optimization With an Improved Pheromone Model for Solving MTSP With Capacity and Time Window Constraint," *IEEE Access*, vol. 8, pp. 106872-106879, June 2020, doi: 10.1109/access.2020.3000501.
- [41] J. Yu, R. Li, Z. Feng, A. Zhao, Z. Yu, Z. Ye, and J. Wang, "A Novel Parallel Ant Colony Optimization Algorithm for Warehouse Path Planning," *J. Control Sci. Eng.*, vol. 2020, Article ID 5287189, 12 pages, Aug. 2020, doi: 10.1155/2020/5287189.
- [42] M. S. Semary, M. E. Fouda, H. N. Hassan, and A. G. Radwan, "Realization of fractional-order capacitor based on passive symmetric network," *J. Adv. Res.*, vol. 18, pp. 147-159, July 2019, doi: 10.1016/j.jare.2019.02.004.
- [43] G. Tsimokou, C. Psychalinos, and A. S. Elwakil, "Emulation of a constant phase element using operational transconductance amplifiers," *Analog Integr. Circuits Signal Process.*, vol. 85, no. 3, pp. 413-423, Dec. 2015, doi: 10.1007/s10470-015-0626-8.
- [44] M. H. Khooban, M. ShaSadeghi, T. Niknam, and F. Blaabjerg, "Analysis, control and design of speed control of electric vehicles delayed model: Multi-objective fuzzy fractional-order PID<sup>h</sup> controller," *IET Sci. Meas. Technol.*, vol. 11, no. 3, pp. 249-261, Nov. 2017, doi: 10.1049/iet-smt.2016.0277.
- [45] V. Sharma and S. Purwar, "Non-linear controllers for a light-weighted all-electric vehicle using chebyshev neural network," *Int. J. Veh. Technol.*, vol. 2014, Article ID 867209, 14 pages, Apr. 2014, doi: 10.1155/2014/867209.
- [46] P. Shah and S. Agashe, "Review of fractional PID controller," *Mechatronics*, vol. 38, pp. 29-41, Sept. 2016, doi: 10.1016/j.mechatronics.2016.06.005.
- [47] I. Pan and S. Das, "Kriging based surrogate modeling for fractional order control of microgrids," *IEEE Trans. Smart Grid*, vol. 6, no. 1, pp. 36-44, July 2015, doi: 10.1109/TSG.2014.2336771.
- [48] M. S. Mahmoud, "Fuzzy control, estimation and diagnosis: Single and interconnected systems," *Saudi Arabia: Springer International*, 2018.
- [49] H. bin Duan, D. bo Wang, and X. fen Yu, "Novel Approach to Nonlinear PID Parameter Optimization Using Ant Colony Optimization Algorithm," *J. Bionic Eng.*, vol. 3, no. 2, pp. 73-78, June 2006, doi: 10.1016/S1672-6529(06)60010-3.
- [50] S. Das, I. Pan, and S. Das, "Performance comparison of optimal fractional order hybrid fuzzy PID controllers for handling oscillatory fractional order processes with dead time," *ISA Trans.*, vol. 52, no. 4, pp. 550-566, July 2013, doi: 10.1016/j.isatra.2013.03.004.
- [51] S. Kapoulea, C. Psychalinos, and A. S. Elwakil, "Realizations of simple fractional-order capacitor emulators with electronically-tunable capacitance," *Integration*, vol. 69, pp. 225-233, Nov. 2019, doi: 10.1016/j.vlsi.2019.04.004.
- [52] S. A. Tekin and M. Alçi, "Design and applications of electronically tunable floating resistor using differential amplifier," *Elektron. ir Elektrotehnika*, vol. 19, no. 4, pp. 41-46, Mar. 2013, doi: 10.5755/j01.eee.19.4.1310.
- [53] Q. Huang, Z. Huang, and H. Zhou, "Non-linear optimal and robust speed control for a light-weighted all-electric vehicle," *IET Control Theory Appl.*, vol. 3, no. 4, pp. 437-444, Apr. 2009, doi: 10.1049/iet-cta.2007.0367.
- [54] P. Anantachaisilp and Z. Lin, "Fractional Order PID Control of Rotor Suspension by Active Magnetic Bearings," *Actuators*, vol. 6, no. 1, pp. 1-31, Jan. 2017, doi: 10.3390/act6010004.
- [55] A. Xavier, R. Irudayaraj, S. Member, N. Izzri, and A. Wahab, "A Matignon's Theorem Based Stability Analysis of Hybrid Power System for Automatic Load Frequency Control using Atom Search Optimized FOPID controller Integral minus Proportional

- Derivative," *IEEE Access*, vol. 8, pp. 168751-168772, Sept. 2020, doi: 10.1109/ACCESS.2020.3021212.
- [56] D. Qian, C. Li, R. P. Agarwal, and P. J. Y. Wong, "Stability analysis of fractional differential system with Riemann – Liouville derivative," *Math. Comput. Model.*, vol. 52, no. 5-6, pp. 862-874, Sept. 2010, doi: 10.1016/j.mcm.2010.05.016.
- [57] G. Tsirimokou, A. Kartci, J. Koton, N. Herencsar, and C. Psychalinos, "Comparative Study of Discrete Component Realizations of Fractional-Order Capacitor and Inductor Active Emulators," *J. Circuits, Syst. Comput.*, vol. 27, no. 11, pp. 1850170 (1–26), Oct. 2018, doi: 10.1142/S0218126618501700.



**MARY ANN GEORGE** (Student member IEEE) was born in India, 1991. She received the Bachelor's degree in Electronics and Communication Engineering (ECE) from Manipal Institute of Technology (MIT), Manipal Academy of Higher Education (MAHE), Karnataka, India, in 2013 and a Master's degree in Digital Electronics and Advanced Communication from MIT, MAHE, Karnataka, India in 2016.

Presently, she is pursuing her Ph.D. in the ECE department, MIT, Manipal. Her research interest includes Fractional-order controllers, Fractional-order systems, and Analog circuits.

Ms. George is a life member of the Indian Society of Systems for Science and Engineering (ISSE).



**DATTAGURU V. KAMAT** (Senior Member IEEE) was born in India, 1965. He received the BE (Electronics and Communication) and ME (Digital electronics) degrees from B.V. Bhoomreddi College of Engineering, Karnataka University, Dharwad, in 1987 and 1997.

He obtained his Ph.D. degree in Analogue VLSI Signal Processing from Manipal Academy of Higher Education (MAHE), Manipal, India, in 2013. He is currently working as a Professor in the Department of Electronics and Communication Engineering, Manipal Institute of Technology, Manipal. The research contribution includes one US patent granted at WIPO, more than twenty full regular papers published in indexed international journals, twenty indexed international conference publications. His research interest areas include Digital, Analog, and Mixed-Signal VLSI design, Analog VLSI Signal Processing, Digital VLSI architectures, and Fractional-order circuits.

Dr. Kamat is a member of IET, IE (India), and ISTE (India).



**CIJI PEARL KURIAN** (Senior Member, IEEE) was born in India, 1964. She received the B.Tech. degree in electrical and electronics engineering from Calicut University, in 1986, the M.Tech. degree in lighting science and engineering from Mangalore University in 1994, and a Ph.D. degree in electrical engineering from Manipal University, Manipal, India, in 2007.

Since 1987, she has been teaching with the Electrical and Electronics Engineering Department, Manipal Institute of Technology, Manipal, a constituent institution of Manipal Academy of Higher Education, India. Her research interests include lighting controls-technology and applications.

Dr. Kurian is a Fellow of the Institution of Engineers India and a Life Member of professional bodies, Indian Society of Lighting Engineers, Indian Society for Technical Education, and Systems Society of India.